J.-P. Parmantier, F. Issac,
V. Gobin
(Onera)

E-mail: jean-philippe.parmantier@onera.fr

Indirect Effects of Lightning on Aircraft and Rotorcraft

This article discusses issues related to indirect lightning on aircraft/rotorcraft. The standard waveforms used for qualifying the vulnerability of a system are introduced, with their frequency spectrum. The identification of the elementary EM coupling phenomenon allows the understanding of the key drivers of the current distribution and field scattering on a complex structure. The system level EM coupling analysis starts with examples of cable-measurements on real aircraft/rotorcraft, from which simple models are derived in order to understand the origin of the resulting waveforms. Various ways of protection are then proposed, ranging from passive to active solutions. Finally, despite limitations, 3D EM modeling is presented as an efficient complement to scale-one tests. The article concludes on the validity of current knowledge on indirect lightning for future aircraft designs.

Introduction

When lightning strikes an aircraft/rotorcraft (AC/RC), the system can be described by two conduction lightning channels made up of a positive leader and a negative leader [1]. From an electrical circuit point of view, the positive channel can be seen as the connection injecting charges at an injection point on the AC/RC whereas the negative channel can be seen as the path for evacuating the charges from an exit point of the AC/RC. “Indirect lightning effects” is thereby the dedicated term used to describe the electromagnetic (EM) effects following a “direct lighting” strike. When a direct lightning strike occurs, a large-amplitude current is injected at the point of injection. In addition to the local mechanical-effects and thermal-effects observed at the injection point, the electric current then circulates over all electrically conducting parts of the structure, on its external surfaces and inside the inner parts, including its electrical system, in order to reach the exit point. Such current redistributed over the entire structure is called the “induced” current. This redistribution of the current is a function of the impedances encountered along the various current paths. Since the current waveform is a transient, the impedances are made up of both a DC part (resistance effect) and a time-varying impedance (inductance).

Consequently, we can identify three main effects that are relevant, from the indirect lightning effects:

- Thermal effects: although the most important damages in terms of mechanical and thermal effects are due to the direct effect, indirect lightning can itself produce such effects. Indeed, on its way towards the exit point, the induced current may be obliged to concentrate along some narrow paths and produce heating of the mechanical parts supporting this current concentration.
- Electric discharges: when circulating along resistive and inductive paths, the electric potential varies on all the parts of the system. Large potential differences may be observed between very close paths, thereby resulting in an electric field that is large enough to overcome the electrical breakdown threshold and thereby produce electrical discharges. Such discharges may be observed at rivets or junctions between material parts and are particularly dangerous when they occur in fuel tanks.
- Effects at electronic equipment levels: a potential difference applied on impedant systems acts like source terms, driving induced currents along cables up to the level of the equipment connectors. Such currents may result in mechanical and thermal effects but, more generally, they result in dysfunction of electronic equipment. This explains why such an effect is categorized as an EM effect and why it is a central matter for the discipline of Electromagnetic Compatibility (EMC).

Of course the AC/RC industry has been coping with indirect lightning for a long time, because it addresses safety issues, this is why it is part of lightning certification in aircraft environments [2], [3], either at the equipment level [4], sub-system level or AC/RC level [5]. Over the past twenty years, in parallel to AC/RC development programs, several cooperative research projects have addressed this topic, which shows the concern for such a phenomenon in the aircraft industry. Significant progress has been made on the control of

this phenomenon. Among the various projects, we mention hereafter some projects in which Onera has been involved:

• in the late 80s, Onera took the opportunity of using the in-flight experiment on the C160 Transall Aircraft (see paper [6] in this Aerospace Lab. edition), sponsored by the French Defense Agency ("Délégation Générale pour l'Armement" – DGA), to instrument some EM field surface sensors on the skin of the aircraft and backdoor sensors behind a carbon composite door. At the time, the bidirectional waveforms were found to be very surprising, but they could be explained by current redistributions calculated on a simplified 3D model of the exterior of the aircraft [7]and backdoor electromagnetic EM coupling could be confirmed by the theory of scattering by small loaded apertures [8].

• in the early 90s, the French DGA pushed the aircraft industry, namely Dassault and Airbus, to work on the understanding of indirect lightning effects. Extensive experimentation was then carried out on a Carbon Composite Wing ("Voilure Composite Carbone" in French, VCC). This experiment set the first basis for the understanding of current redistribution on cylindrical-like two-dimensional (2D) structures [9]. The experiment was then followed by several studies extending the 2D approach to the three-dimensional (3D) redistribution effects.

• in the 90s, the European Union (EU) launched two major projects involving Academic, laboratory and industry partners, in which indirect lightning had a significant place. The FULMEN EU project, as part of the framework project 3 (FP3), established the first basis for the 3D modeling of aircraft, as well as its interior [10], [11] including wiring. It was followed by the 5th framework EMHAZ project, which took this analysis a step further by using more complex geometries. After these projects, the 3D modeling of indirect lightning on AC/RC became increasingly usual in AC/RC industry qualification and certification processes.

• from 2005 to 2008, the MOVEA French project, again sponsored by the French DGA, had the ambition of building an AC/RC model to calculate both the EM constraints generated by indirect lightning on an AC/RC, as well as to assess the possible disruptions observed at the level of the equipment [12]. In this project, an extensive analysis of the AC/RC experimental database was carried out, considering the AC/RC wiring as a deployed sensor of indirect current redistribution on AC/RC. Such an analysis investigated and explained in which geometrical configurations, and why, large induced currents could be observed on an AC/RC.

The purpose of this article is to review the fundamental bases, in order to be able to capture the relevant physics of indirect lightning on AC/RC. With this, the reader will understand how indirect lightning becomes a source of induced currents and how those induced currents may be distributed over AC/RC systems. With various types of modeling approaches, it aims at understanding the EM physics that drives indirect lightning induced current waveforms and distribution.

In § "Time domain waveforms and frequency spectrum", we briefly recall the time domain waveforms involved in the indirect lightning process, with their associated frequency spectra. First we introduce the waveforms as they appear in a standard indirect lightning current sequence. Then, we explain the interest in simulating these waveforms as biexponential-like waveforms and how to make this analogy. In § "Elementary EM effects", we present the elementary EM effects that contribute to the overall EM coupling indirect lightning response on a 3D structure. For this, we make the distinction between conduction and scattering effects. Conduction effects are EM effects characterized by the circulation of currents, as a function of the impedance that they encounter: 3 main signatures are considered, DC resistance, frequency varying impedance and current redistribution effects. These signatures are explained with simple analytical calculations and 2D-wire invariant-geometry models. Particularly, current redistribution is demonstrated with a 3D calculation of the surface current on an airplane model and an airplane payload model. A lightning EM scattering related effect is introduced with the problem of small apertures (small compared to the wavelength), for which efficient electric and magnetic dipole models can be derived. This approach logically leads us to the model of loaded apertures, applied in order to describe the field emission produced through materials and at the junction levels. Throughout the chapter, we make a comparison of the influence of the various elementary effects when they happen to be combined.

§ "Indirect lightning EM effects at system level" addresses the problem of effects at the electrical-system level; therefore we introduce here the problem of EM coupling in cables. First, we display some A-waveform induced currents measured on real aircraft and we identify typical frequency variation signatures of the transfer functions between current in wires over total injected currents. Then, in order to analyze the origin of those signatures, we use 2D-invariant models, such as the models considered in § "Time domain waveforms and frequency spectrum". Starting from a simple cylinder shape structure with internal wires, we progressively introduce a more realistic cross-section geometry encountered on a real helicopter. This analysis allows Thevenin-like equivalent source models to be derived, including a voltage generator and associated impedance. The common-mode type of coupling generated by currents flowing over lossy structures is thereby introduced. Finally, we investigate the relevance of the linear approximation by analyzing cable response on a helicopter with different amplitudes of the injected current. A large part of the material in this chapter comes from the MOVEA project previously mentioned [12].

§ "System level indirect lightning protection" introduces the problem of protection against indirect lightning effects. The protection comprises passive protection, which uses the installation of the structure and the system for designing as many shields as possible to decrease the internal EM coupling constraints, and active protection, which acts directly at the level of the equipment parts or electronic systems. The presentation focuses on passive protection concepts and goes through topology-based measures, such as grounding and bounding, cable shielding and cable routing. The shielded-cable part offers the opportunity to introduce the shield transfer impedance concept as a particular application of the EM shielding theory. Active protection mainly considers protection based on equipment inputs, with active non-linear devices triggered by the induced current, which is not considered in this paper because it is very specific to the type of functional signals to be protected. In addition, the specific protection problem of fuel tanks is not addressed in this article, even though its origin is clearly an indirect lightning problem. The reader will find a description of this specific problem [13]. Because of the possible damaging consequences on the mechanical structure, this problem is handled together within the direct lightning effects.

§ "System level numerical simulation" concerns a system level numerical simulation, since we consider that this topic has now become an integral part of any lightning design or analysis process on AC/RC. Based on 3D models capable of solving Maxwell's equations, or some of their approximations, we begin to introduce the specificities related

to indirect lightning and identify real difficulties in building and solving the models. As a demonstration of the progress made on modeling issues, particular emphasis is placed on the recent work by Dassault in the calculation of indirect lightning response, on their F7X airplane, with a degree of complexity that does not seem to have been achieved so far, to our knowledge. The use of stick models is also presented as an old trend recently put again to the fore, with much lighter models than 3D full-wave solvers.

Finally, after a summary of the main lessons of this article, we conclude on the consequence of new system designs, for which it may no longer be possible to separate direct and indirect lightning analysis, as is usually done in current practice.

Time domain waveforms and frequency spectrum

Standard waveforms

The signature of lightning injection current is not reproducible from one event to another, but typical signatures can be observed on all the events. This is why normalization standards have tried to define generic waveforms with which systems must comply [14], [5]. For AC/RC, the RTCA [4] and EUROCAE [15]define the waveform sequences represented in figure 1 and figure 2 ([4], [15]). Figure 1 constitutes the main standardized waveform sequence. The entire waveform is constituted by 4 subsequent elementary waveforms, each having a large action integral. The action integral is defined by the integral of the square of the current waveform; it is thereby related to the energy of the signal. Large action integrals thereby characterize large current amplitudes or long persistence time of their waveform. The 4 elementary waveforms are:

- Waveform A, which is a pulse representing the first arc. It has the largest amplitude of all of the elementary lightning waveforms (200 kA) and a duration of about 500 μs;
- Waveform B is the intermediate pulse current waveform making the slow transition between the waveform A impulse waveform starting from 2 kA and the constant C waveform (figure 1) at a level between 200 and 800 A, on a time scale ranging from 500 μs to 500 ms;
- The C waveform is a constant current representing the persistent current phase (between 200 and 800 A). This phase extends between 500 ms and 1s;
- The waveform D is another impulse waveform representing the second arc with a maximum equal to half of the maximum of the A waveform during 500 μs.

Note that all of the levels defined here correspond to a first arc waveform maximum scaled at 200 kA, which corresponds to the worst case, defined as 1% of all of the current waveforms on aircraft. Usual maximum amplitudes corresponding to 90% of the events have a maximum of the first arc of about 30 kA [16].

In addition to these main waveforms, the RTCA [4] and EUROCAE [15] define repetitive waveforms (the levels defined hereafter are scaled with respect to a 200 kA first arc amplitude waveform). The first type of waveform is the so called “multiburst waveform” (figure 2-a), which corresponds to the phase, in which the lightning channel is not totally established and which occurs before the first arc phase presented in figure 1. The RTCA and EUROCAE waveforms define it as 24 groups of 20 pulses occurring between 10 μs and 200 μs. Each elementary pulse is a called an H waveform, with an amplitude of 10 kA.

A second set of repetitive waveforms correspond to the so-called return stroke phenomenon (figure 2-b). The RTC and EUROCAE standards define it as a series of 24 half-amplitude D waveforms occurring during 2s, every 10-to-200 ms.

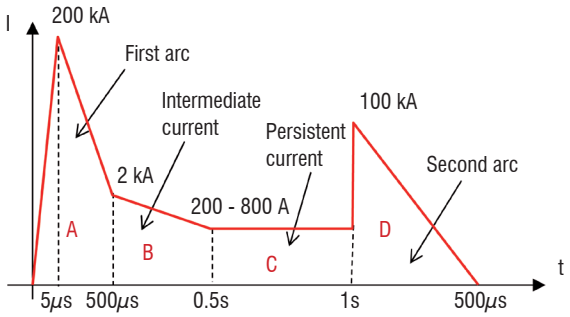

Figure 1 - Typical arc lightning waveform, as defined in the RTCA [4] and EUROCAE [15]

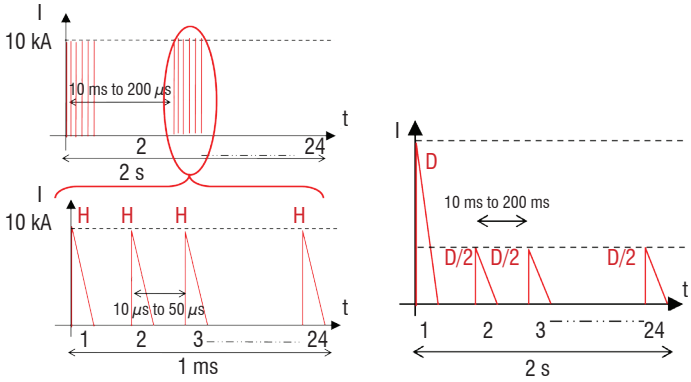

a) Multiple burst waveform (H waveform)

b) Multistroke waveform

Figure 2 - Typical repetitive lightning waveforms, as defined in the RTCA [4] and EUROCAE [15]

Simulation of the standard waveforms

In theory, the standard waveform defined by RTCA and EUROCAE are the ones to be shown by AC/RC airframers. Nevertheless, the test laboratories are not able to generate the set of pulses shown in figure 1 and in figure 2 in sequence. They generally can show, one at a time, some of the elementary waveforms independently and, sometimes, the sequence of two or three of the waveforms, however not necessarily in the right order of occurrence. The main elementary waveforms of lightning current for AC/RC indirect lightning certification are impulse A and H waveforms and, to a smaller extent, D and B waveforms.

Thus, the question is now: how can such pulses be generated with the given rise and decay times and the maximum amplitude? The biexponential waveform provides a very efficient and simple generic mathematical model for all of the elementary waveforms, because they are very close to the waveforms generated by real current sources, generally based on capacitive discharges [17], [18], [15].

The biexponential waveform is defined mathematically by the difference between two decaying exponentials:

$$I(t) = I_o\left(e^{-\alpha.t} - e^{-\beta.t}\right) \quad (1)$$

where α and β are two constant numbers in s^{-1} and I_0 is a constant number in Amperes.

A typical biexponential waveform is represented in figure 3. Its main characteristics are defined as follows:

- Amplitude of the maximum, Imax:

$$I_{max} = I_o\left(K-1\right).K^{\frac{-K}{K-1}} \quad (2)$$

with

$$K = \frac{\beta}{\alpha} \quad (3)$$

note that for $\beta >> \alpha$, $I_{max} = I_0$

- Rise time, T_r, defined as the time difference that exists when the signal rises up from 10% to 90% of its maximum amplitude:

$$T_r = \frac{2.19}{\beta}(s) \quad (4)$$

- Decay time, Δ, defined as the time difference for which the rising waveform and the decaying waveforms are equal to half of the maximum.

$$\Delta = \frac{0.69}{\alpha}(s) \quad (5)$$

Note that the exponential is not the only waveform for approximating the pulse. Especially, the biexponential has a non-zero derivative at time zero which is not physical and may cause problems in models. Other waveforms can be used in order to avoid this drawback [19].

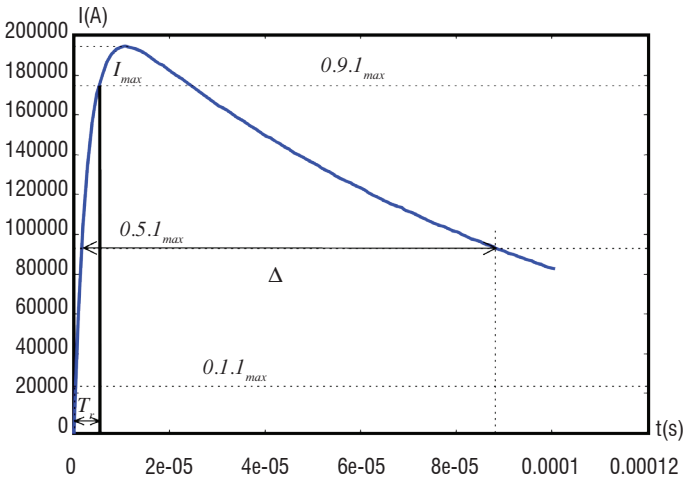

Figure 3 - General biexponential waveform and associated characteristics

Table 1 presents the characteristics of the A, B, D and H waveforms from RTCA and EUROCAE (see Video 1 "Standard lightning waveforms and general lightning current sequence"). Figure 4 zooms in on the first instants of those waveforms, whereas figure 5 displays their frequency spectra. The Fourier transform of the biexponential waveform defined in (1) is equal to:

$$E(f) = \frac{1}{\left(\alpha + j.2\pi f\right).\left(\beta + j.2\pi f\right)} \quad (6)$$

It shows two cut off frequencies f_{c1} and f_{c2} respectively defined by:

$$f_{c1} = \frac{\alpha}{2\pi} \quad (7)$$

and

$$f_{c1} = \frac{\beta}{2\pi} \quad (8)$$

On the one hand, f_{c1} depends on the α coefficient whose inverse defines the decay time, that is to say, the long times of the waveform. On the other hand, f_{c1} depends on the α coefficient whose inverse defines the rise time and is therefore related to the early times of the waveform. Figure 4 and figure 5 clearly show that the B waveform is a slow waveform (frequency content lower than some hundreds of Hz), with a quite large action integral (the integral of the waveform is equal to the Fourier transform at the frequency zero). The A waveform is also a slow waveform with a long rise time and a frequency content lower than some kHz, but with a large energy content (the largest of the 4 waveforms). Waveform D is very similar to waveform A for late times, with an amplitude divided by two. However, the rise time is somewhat larger than the rise time of the A waveform (see also the second cut-off frequency, which is larger than the second cut-off frequency for the waveform A). Finally, the H waveform is the least energetic waveform with the largest frequency content, with a first cut-off frequency of about 100 kHz.

Finally, compared to the usual waveforms considered in EM environments, such as Electromagnetic Pulse (EMP) or High Intensity Radiated Fields (HIRF), it appears that lightning is a low frequency phenomenon. Nevertheless, we will see later on in this document that its frequency content applied on large structures is large enough to generate all types of typical induced EM responses, such as inductive effects, field scattering and wave propagation.

	Waveform A	Waveform B	Waveform D	Waveform H
$Io(A)$	218810	11300	109405	10572
$\alpha(s^{-1})$	11354	700	22708	187191
$\beta(s^{-1})$	647265	2000	1294530	19105100
t_m	0,5 ms	10 ms	1 ms	10 μs
$I_{max}(kA)$	200	5	100	10

Table 1 - α and β coefficients and main characteristics of the impulse [4] and [15] biexponential waveforms

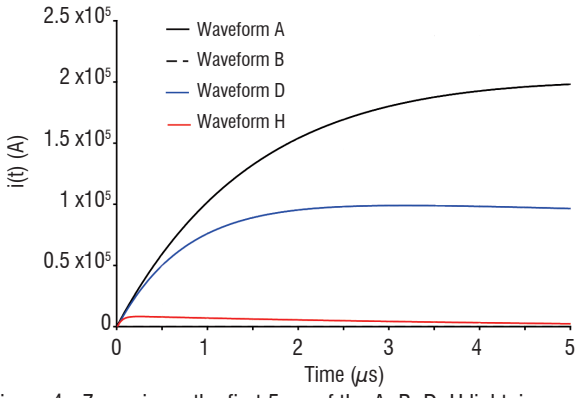

Figure 4 - Zoom-in on the first 5 μs of the A, B, D, H lightning waveforms

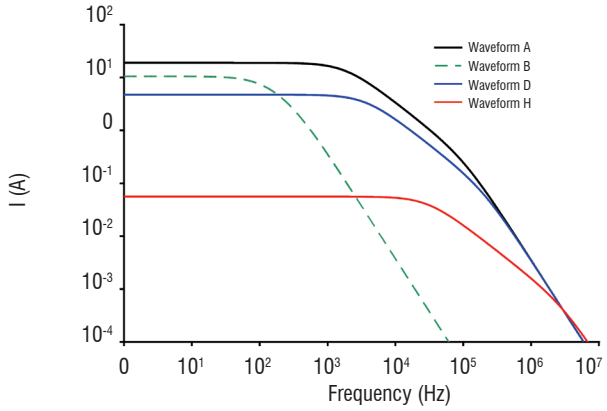

Figure 5 - A, B, D, H lightning waveform frequency spectra

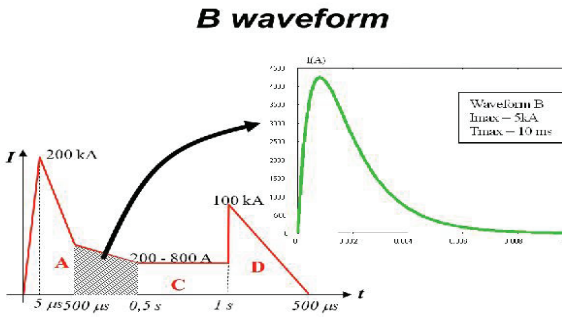

Video 1 - Standard lightning waveforms and general lightning current sequence
http://www.aerospacelab-journal.org/al5/indirect-effects-of-lightning-on-aircraft-and-rotorcraft

Elementary EM effects

We will now concentrate on the EM physics, which characterizes EM coupling on structures likely to be encountered on AC/RC. In particular, we will consider linear effects and assume that the sources triggering those effects do not generate any non-linearity. The physics involves several EM effects of specific nature that we will consider separately, under the name of “elementary effects”. In order to reveal those effects separately we will consider EM coupling situations on generic structures. This simplification restriction will allow us to make the distinction from the so-called “system-level effects”, which will be the subject of the next chapter.

Conduction effect

The conduction effect is related to the injection of an electric current inside the materials that constitute the system. We will distinguish 2 main phenomena:

- the resistance effect, which is a DC or very low frequency phenomenon that only depends on the electric conductivity of materials and therefore on their DC resistance;
- the redistribution effect, which is a dynamic phenomenon involving higher frequencies and depending on the geometry of the structure, and therefore on their frequency-varying impedance.

DC resistance

We will first consider the DC regime, or a regime for which the current can be considered as homogeneous inside a cross-section geometry of a material. With such an approximation, we will see after that we can consider the material as “thin” with respect to so-called “diffusion” effects related to the "skin effect". Let us consider the piece of rectangular material presented in figure 6 (length l, width w and depth d), in which a current I is injected. Assuming a uniform current density in the section of the sample, the resistance is classically given by [20]:

$$R = \frac{\ell}{\sigma S} = \frac{\ell}{\sigma w d} \qquad (9)$$

where σ is the electric conductivity and S is the section of the material at the current injection point, d being the thickness and w the width.

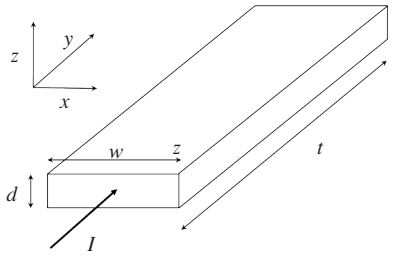

Figure 6: Rectangular material used to demonstrate resistance effects

This resistance concept, well known in electrical circuit theory, can also be derived from EM considerations involving the total tangential electric field Et on the material [8]. Indeed, the surface impedance of a material is defined as the ratio between Et and the homogeneous surface current density of the surface, J_s:

$$Z_s = \frac{E_t}{J_s} = \frac{1}{\sigma . d} \qquad (10)$$

We see that the surface impedance can be also evaluated as the resistance of a square material $(w=l)$. Whereas the resistance definition depends on the size of the material, the surface impedance is characteristic of the material with a given depth, whatever its surface dimensions are. This definition only assumes the homogeneity of the currents in the depth of material (no "skin effect").

Table 2 gives typical values of materials encountered on aircraft. The reference value is the value of the aluminum sheet for which we have a Z_s value calculated from (10) with the theoretical conductivity and the depth. For carbon materials, an equivalent conductivity is obtained from (10). For the two proposed materials used for direct lightning effect protection (copper foil and bronze mesh), only the measured Z_s value is available. In the case of application of those protections on carbon composite materials, the two Z_s values will act in parallel and will of course significantly improve the Z_s.

Type of material	Depth	Conductivity $(\Omega.m)^{-1}$	$Zs(m\ \Omega)$
Aluminum sheet	$10\ \mu m$	$37.6\ 10^{+6}$	2.7 *
Carbon panel (fabric 3 folds)	$900\ \mu m$	$1.5\ 10^{+4}$ *	72
Carbon panel	3 mm	$3.0\ 10^{+4}$ *	11
Expanded copper foil			2
Bronze mesh			6

Table 2 - Typical surface impedance materials (*Calculated)

Box 1 - The Z_s probe: an efficient non-intrusive device for in-situ Z_s measurement of materials

A direct evaluation of the surface impedance with an impedance-meter presents several practical drawbacks:

- This method necessarily adds parasitic junction resistances to the sample under test. They can be due to the additional metal pieces that must be used in order to control the flux of the injected currents;
- It is not compatible with aeronautical in-situ measurements, the material under test being generally not isolated from other parts of the structure and also covered with protection paint, for example.

A "Z_s probe" has been designed at Onera [8] to overcome these restrictions. The main idea is to create no-contact "Foucault currents" inside the material by an illuminating source, these induced currents being related to the impedance of the material (the higher the resistance, the smaller the currents). The completion of the injection probe with a reception probe can give access to the value of the Zs surface impedance.

An appropriate application of this principle is obtained with 2 parallel circular emitting and receiving loops. After a calibration of the coupling, in free space and for a selected band of frequencies, a sample is introduced between the loops (figure B1-1a); the circular induced current being negligible at low frequency and of increasing magnitude for higher frequencies (see numerical simulation in figure B1-1b), the variation of the coupling, in the same frequency band happens to be quite well approximated by a first order filter function for optimized geometrical parameters of the device (figure B1-1c).

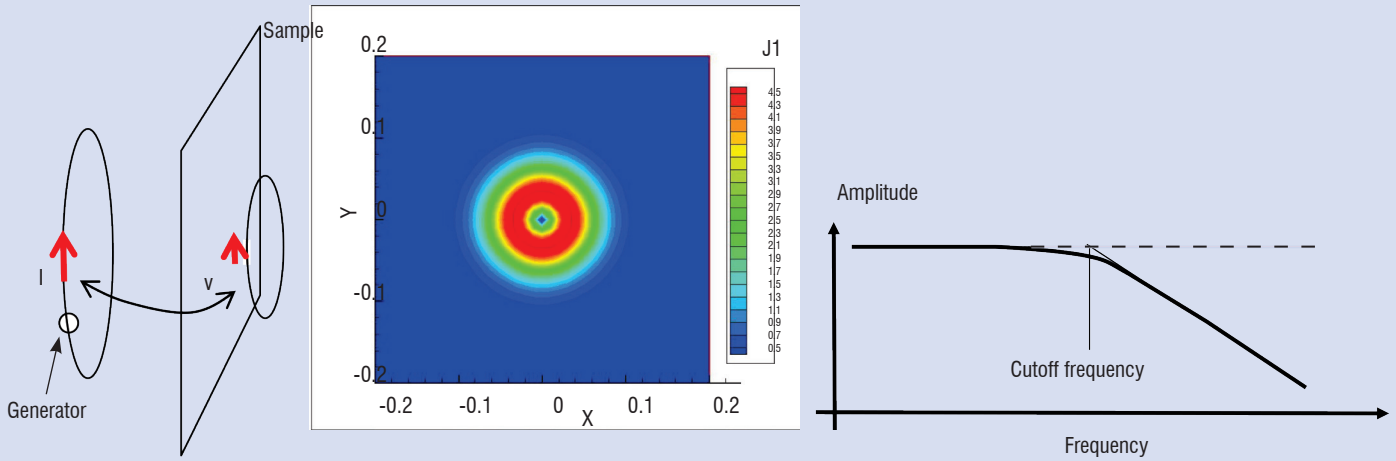

a) Measurement Principle b) Currents developed on the sample c) Transfer function between the two loops (log-log scale)

Figure B1 - 1: Zs probe main features

The measured cut-off frequency is proportional to the impedance of the sample if the material is isotropic and homogenous (typically on a 20 cm x 20 cm surface). Impedances of between a few mOhms to a few Ohms are within the application scope of the technique. The method appears to be efficient to characterize thin metal materials or carbon fiber composite materials, if the fibers are oriented in enough directions (giving rise to an almost planar isotropy).

A variation of the method, with both loops on the same side of the sample, is applicable for material covered by a thin layer of paint and allows application of the technique as a non-intrusive probe directly applicable in-situ.

Frequency varying material resistance

Now, let us consider some higher frequencies, which give rise to another type of EM physics called the “skin effect” [20]. When a material is illuminated by an EM wave, the EM fields penetrate the material; this phenomenon is known by the term “diffusion”; the skin effect is the phenomenon that tends to concentrate the currents on the illuminated side of the material. The distribution of the current density J being exponential in the material, $J=J_s e^{-d/\delta}$, the skin depth is defined as the depth δ for which the surface current density at the surface J_s is divided by e. δ is therefore the depth at which approximately 63% of the current is concentrated. It is defined as:

$$\delta = \frac{1}{\sqrt{\mu\pi\sigma f}} \qquad (11)$$

where μ is the magnetic permeability of the material.

The more the frequency increases, the more δ decreases and the more the resistance increases.

From an EM point of view, the skin effect, by participating in the attenuation of the current inside the material, contributes therefore to the shielding of the magnetic field. It is also at the origin of the frequency

variation of the transfer impedance of shielded cables (see § "Protection with shielded cables").

Current redistribution

At high frequencies current lines tend to repel each other, due to inductive effects. Therefore, the more the frequency increases, the more the current will distribute over the far dimensions of the object, that is to say, the edges and the corners of the structures. This phenomenon thereby depends on the geometry of the structure, unlike the resistance effects seen before, which only depended on the nature of the material.

The skin effect can be seen as a particular case of the current redistribution. In this case, the current is redistributed in the depth of the material. If the material is a plate, as described in the box 2, the current will concentrate on both sides of the material. If the material is part of a closet or a structural metallic surface, the current will concentrate on the external surface of the material.

Box 2 - Current redistribution on a plate

A simple way to describe the current lines is to use a thin wire approximation. This type of approximation will be more extensively used in the following sections (see § "Indirect lightning EM effects at system level").

In figure B2-1a we present the problem of lossy conductive plate on which a current Itot is injected, according to the medium axis of symmetry of the plate. In our case, we are more interested in the distribution of the currents at the center, Icen, and on the edges, I_{ext}. In figure B2-1b we present a rough (but convenient) thin wire approximation of the problem. The 3 currents, Icen and Iext are supported by 3 thin wires connected together at the ends.

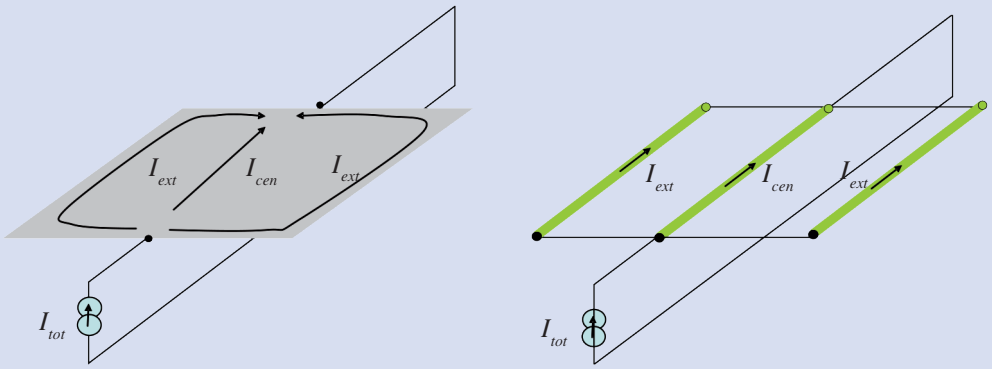

a) Problem to solve b) Thin wire model

Figure B2-1: Thin wire modeling of a metallic plate on which a current is injected

The analytical resolution of such a problem can be performed by solving the equivalent electrical circuit. As for every thin wire model approximation, the equivalent circuit can be described in a matrix form relating the various currents to the voltage drop V between the two sides of the plates. The relation between the currents on the wires and V is provided by an impedance matrix that includes the following terms:

- the resistances of each wire equal to R because the 3 wires are identical (the 3 wire resistances in parallel must be equal to the DC resistance of the plate);
- the self-inductances of each wire. Because our 3 wires are chosen to be identical, the 3 inductances are equal to L;
- the mutual inductances between the wires. Those mutual inductances depend on the geometry of the wires and the distance between them. Because of the symmetry of the problem, two types of mutual inductances must be distinguished:
  - M, the 2 mutual inductances between the center conductor and the 2 edge conductors
  - m, the mutual inductance between the two edge conductors

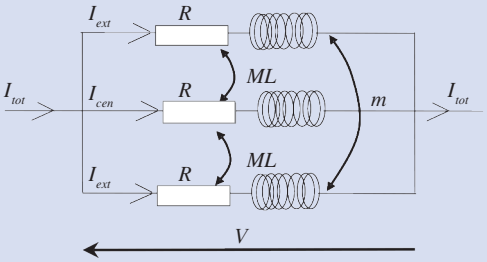

Figure B2-2: Equivalent circuit of the 3-thin-wire conducting plate model in figure B2-1

Finally, the three equations of the matrix equation can be simplified to the following 2 equations:

$$\begin{cases} V = \left[R + j\left(M + m\right).\omega \right].I_{ext} + jM\omega.I_{cen} \\ V = 2\,jM\omega.I_{ext} + \left(R + jL\omega\right).I_{cen} \end{cases} \quad (12)$$

with:

$$I_{tot} = 2.I_{ext} + I_{cen} \quad (13)$$

The resolution of (12) with (13) gives:

$$I_{cen} = \left(1 - \frac{j\omega\left(M - m\right)}{R + j\omega\left(L - M\right)} \right).I_{ext} \quad (14)$$

with $M > m$.

The analysis of (14) gives the following information:

1. At DC ($\omega = 0$), $I_{cen} = I_{ext}$, The current is uniformly distributed
2. At high frequencies (when imaginary parts become much larger than real parts):

$$I_{cen} = \left(1 - \frac{\left(M - m\right)}{L - M} \right).I_{ext} \quad (15)$$

which implies that $I_{cen} < I_{ext}$. The current is lower at the center than on the edges. Of course, as indicated before, this result is a rough approximation, because the model is limited to 3 wires. The model becomes much more precise when the number of wires increases and the model allows the progressive decrease of the currents in the wires from the edges to the center to be shown.

Video 2-a, Video 2-b and Video 2-c illustrate the redistribution effect on a 3D generic structure. Here, the example is a model of a Transall aircraft in various configurations of injection and output points of the current. Those injection and output points are defined from a zoning analysis, as described in [21], [22]. The calculation has been made with the ALICE Finite Difference Time Domain (FDTD) code from Onera. The model is very simple and its only intent is to visualize how the currents will circulate on the 3D surface. Several important elementary effects previously described must be noticed on these animations:

• The redistribution effect, which concentrates the currents on the edges. This effect occurs in the early time of the current injection because the frequency content is maximum. On the wings or on the tail for example, the current is distributed on the edges, whereas on the fuselage, which is close to a circle, the current is almost equally distributed. After the occurrence of the maximum of the current, the current vanishes uniformly on the surface between the injection and the exit points.

• The search for an exit point. The current flows along the minimum impedance path. In the early time, this impedance is mainly inductive. This is why the current may flow in parts of the 3D geometry that are not in the direct path between the injection and the exit point. The phenomenon looks as though the current were seeking its path, from the injection point to the exit point.

• The absence of resonance effects. The size of the aircraft and the frequency content of the A waveform are too small to excite resonances that would appear as currents bouncing back and forth between two geometrical points. On such an object, resonances would be of $l = \lambda/2$, where l is a characteristic dimension of the object (fuselage length or distance between wings, for example) and λ is the smallest frequency of the frequency spectrum. Such resonances are unlikely to occur on usual commercial aircraft in operation at this time, except perhaps for H waveforms on large AC such as Boeing 747 or A380.

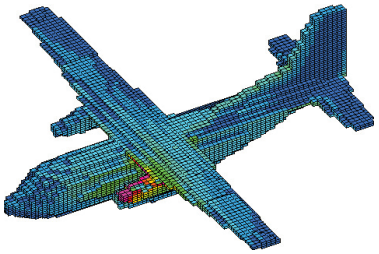

a) Configuration “Engine to tail”

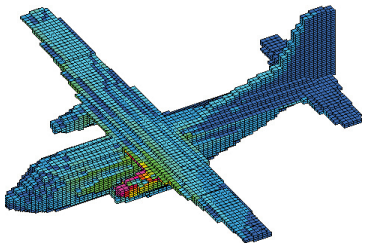

b) Configuration “Engine to Wing”

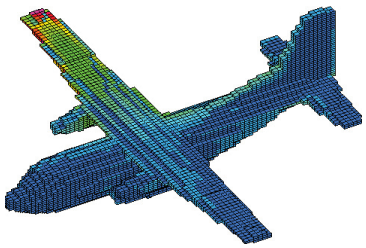

c) Configuration “Wing to Tail”

Video 2 - A waveform lightning injection on a Transall Aircraft
http://www.aerospacelab-journal.org/al5/indirect-effects-of-lightning-on-aircraft-and-rotorcraft

Video 3 presents another animated picture, still calculated with ALICE's FDTD computer code from Onera. It concerns the A waveform lightning injection on the AASM guided bomb developed by SAGEM defense (SAFRAN group) [23]. The first configuration in video 3 a presents the "free-flight" configuration, for which the current enters the bomb at the level of its "guiding kit" in front and exits at the level of its "propulsion kit" at the rear (the animation does not show the damping times but stops at the time of the maximum current). Due to the cylindrical shape of the bomb, the redistribution effect only occurs at the levels of the winglets. Note also some points of intensification of the currents. which consist in obliged paths of circulation of currents at the level of peripheral screws between the guiding kit and the bomb core. Video 3 b consists in an injection on the guiding kit of the bomb and an exit point on the wing of the aircraft. The movie clearly shows the redistribution of the currents on the edges of the wing. Finally, video 3 c shows an injection exit point configuration similar to the "free flight" configuration, but when the bomb is attached to the wing. This time, we see the low impedance path-search phenomenon for which the current flows to the wing before coming back to the exit point, which is at the rear of the AASM. Such a phenomenon gives rise to bipolar time domain surface current signatures, for which the currents flow in two directions at a given observation point on the surface of the object.

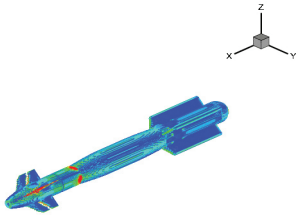

a) Configuration "AASM – AASM" in free flight

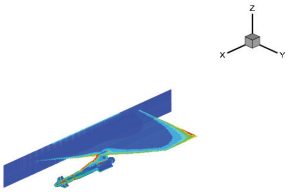

b) Configuration "AASM – wing"

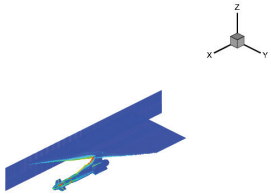

c) Configuration "AASM – AASM"

Video 3 - A lightning waveform injection on the AASM system – Courtesy SAGEM defense
http://www.aerospacelab-journal.org/al5/indirect-effects-of-lightning-on-aircraft-and-rotorcraft

EM scattering effect

In EM coupling theory, "scattering" is the term reserved for the generation of EM fields due to an obstacle in the path of the current on a structure. This is typical physics used on purpose for building antennas. As far as EM coupling is concerned, the radiation of the EM fields is not intentional: EM field scattering is mainly due to the presence of windows or doors, which behave as "apertures". Some of those apertures may be transparent from and EM point of view; they are called "free" apertures. Some are closed with non-transparent materials; they are called "loaded" apertures. This is typically the case of bay-doors on AC/RC.

Besides, we have seen that lightning is a low frequency phenomenon. If we consider 1 MHz as the very maximum frequency of any type of lightning waveform, the wavelength is equal to 30m, which makes any type of aperture encountered on an aircraft behave as a so-called "small aperture". Indeed, the small aperture theory is particularly well suited for lightning waveforms.

Free small apertures

The theory of small apertures allows a very convenient approximation. When an aperture is illuminated by an incident field (this incident field having been produced by a current injection on the structure, for example), it can be shown [24] that the radiation of the field due to the aperture is equivalent to the combined radiation of a magnetic dipole of moment, $\vec{P}_m$, and an electric dipole of moment, $\vec{P}_e$:

$$\overrightarrow{P_e} = \varepsilon_o \alpha_e \overrightarrow{E_{se}} \tag{16}$$

and

$$\overrightarrow{P_m} = [\alpha_m].\overrightarrow{H_{cc}} \tag{17}$$

It can be shown that this approximation is valid for a calculation of the fields at a distance larger than the largest dimension of the aperture. The two dipoles depend on two quantities:

• The geometry of the aperture with two quantities called "electric polarizability"α_e (a scalar) and "magnetic polarizability" $[\alpha_m]$ (a 2x2 diagonal tensor). Table 3 gives practical formulas for several shapes of apertures [25]. The circular aperture formulas generally give a good approximation for any shape of apertures, such as windows, whereas the elliptic apertures give good approximation of one-direction extended apertures such as slots;

Shape	α_e	α_{mxx}	α_{myy}
Circle of radius α	$4\frac{\alpha^3}{3}$	$4\frac{\alpha^3}{3}$	$8\frac{\alpha^3}{3}$
Ellipse	$\frac{\pi}{12}\frac{w^2 l}{G(e)}$	$\frac{\pi}{12}\frac{l^3 e^2}{F(e)-G(e)}$	$\frac{\pi}{12}\frac{l^3 e^2}{(l/w)^2 F(e)-G(e)}$
Narrow ellipse	$\frac{\pi}{12}w^2 l$	$\frac{\pi}{12}\frac{l^3}{Ln(4l/w)-1}$	$\frac{\pi}{12}w^2 l$

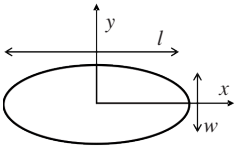

Ellipse dimensions

Table 3 - Polarizabilities of typical apertures (from [25])

with:

$$e = \sqrt{1\left(\frac{w}{l}\right)^2}$$

$$F(e) = \int_0^{\frac{\pi}{2}} \frac{1}{\sqrt{1-e^2\sin^2\theta}} d\theta$$

$$G(e) = \int_0^{\frac{\pi}{2}} \sqrt{1-e^2\sin^2\theta}\, d\theta$$

• The short-circuited incident magnetic fields $\overrightarrow{H_{sc}}$ and electric fields $\overrightarrow{H_{sc}}$ on the aperture, that is to say, the fields that would have been obtained if the aperture were closed by a perfectly conducting material. In [26], it is shown that those surface fields can be measured close to the aperture surface of a 3D structure (they are not significantly modified by the presence of the aperture) and used as source terms for calculating equivalent sources inside a 3D structure. Such short-circuited fields combined to polarizabilities can also be used to directly calculate voltage and current sources induced at the level of a cable running underneath [25]. Note that polarizabilities roughly vary as the cube of the main dimension, which means that the scattered field also follows this cubic variation.

Loaded small apertures

When a small aperture is loaded by a material characterized by its Zs surface impedance, the model of two equivalent magnetic and electric dipoles is still valid, but a frequency variation must be applied on the two free aperture dipoles moments $\overrightarrow{P_{m_o}}$ and $\overrightarrow{P_{e_o}}$ [27], [28]. We have:

$$\overrightarrow{P_m} = \frac{\overrightarrow{P_{m_o}}}{\left(1 + j.\frac{f}{f_m}\right)} \quad (18)$$

with:

$$f_m = \frac{3Z_s}{8\mu_o\alpha} \quad (19)$$

and

$$\overrightarrow{P_e} = \overrightarrow{P_{e_o}}.j.\frac{f}{f_e} \quad (20)$$

with

$$f_e = \frac{1}{16\varepsilon_o Z_s \alpha} \quad (21)$$

Figure 7 shows the electric and magnetic field attenuations for a circular aperture loaded with a $Z_s = 1\Omega$ material (this value is a bad conductivity for usual Carbon Fiber Composite (CFC) materials but is convenient for the normalization of our results). This attenuation is defined as the ratio of the field in the presence of the material over the field without the material. These curves are directly obtained by the ratio between the equivalent dipoles defined in (18) and (20). The electric field attenuation decreases linearly with the frequency. However, for the frequencies concerned by lightning we observe that this attenuation is quite large (more than 80 dBs). On the contrary, we observe that the attenuation of the magnetic field is almost equal to zero up to the f_m cut-off frequency. It is only after this frequency that the attenuation begins. This is a very usual behavior of magnetic fields, which cannot be stopped at low frequencies due to the finite conductivity of materials. This is why, in the continuation of this article, our main concern will be for the penetration of the magnetic field. Nevertheless, the reader must keep in mind that this does not mean that there is no electric field behind the aperture. Because of Faraday's law, the flux of the magnetic field in a closed contour is thereby related to the circulation of the electric field on this contour [29].

Note that the higher importance of the magnetic transfer function vs. the electric transfer function for shields is directly observed for cable shields: to characterize shielded-cables, the transfer impedance of the cable (related to magnetic coupling) is the relevant parameter in general and is available in the data sheets for commercial cables. The transfer admittance (related to electric coupling) is generally neglected and often not mentioned (see box 5).

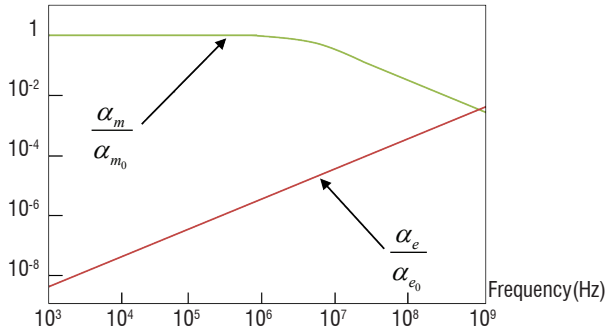

Figure 7 - Electric and magnetic field attenuation for a circular aperture of radius a, loaded by a $Z_s = 1\Omega$ material

Figure 8 shows a shielding effect calculated on a loaded square aperture when a current is injected in the metallic plate supporting the loaded aperture. The calculation is made with an Electric Field Integral Equation (EFIE) solver in the frequency domain. The straight segments represent the flow of the surface current. Their length is proportional to the amplitude of the current. For frequencies lower than f_m, we see that the current flows around the aperture, as if the aperture were free (the currents flow along the minimum resistance path). This deviation of the currents creates the radiation of the EM field. When the frequency is equal to f_m, we see that some part of the current is flowing through the loading material. When the frequency becomes larger than f_m more current is flowing straight across the loading material, thereby providing shielding of the magnetic field.

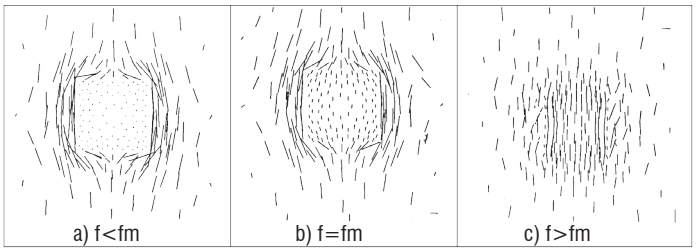

Figure 8 - Magnetic shielding effect on a square loaded aperture (from [8])

The first order filter behavior of the magnetic shielding effect is the universal magnetic shielding rule, which requires current to circulate on a material in order to produce the shielding effect. As a demonstration, table 4 shows that the magnetic cut-off frequencies for geometrical shapes made of a material with a surface impedance Zs_0. f_m is always proportional to Zs_0 and to the inverse of the characteristic dimension of the geometry ("α" in table 4).

Box 3 - EM Scattering versus skin effect

As seen before and related to the skin effect phenomenon, when a volume is closed and lossy with a surface impedance equal to Zs, the EM field enters the cavity by penetrating through the constitutive materials. This diffusion effect produces long time domain waveforms inside the volumes. We can thereby ask ourselves which effect dominates when scattering and diffusion are in competition.
Let us consider a lossy material of depth "e". On the one hand, we can calculate the frequency f_δ for which the skin depth is equal to half of the depth of the material. We find:

$$f_\delta = \frac{4Z_s}{\pi\mu e} \tag{22}$$

(μ is the magnetic permeability of the material). On the other hand, we consider the magnetic cut-off frequency, which characterizes the penetration of the magnetic field through a loaded aperture with the same Zs and diameter D:

$$f_c = \frac{3.Z_s}{8.\mu}.\frac{2}{D} \tag{23}$$

The ratio between these two frequencies gives [30]:

$$\frac{f_\delta}{f_c} = \frac{16}{3\mu} \approx 1,7.\frac{D}{e} \tag{24}$$

This means that, even if the diameter of the aperture becomes equal to the depth of the material, the frequency for which the skin effect begins to be relevant is almost 2 times larger than the frequency after which the magnetic field is attenuated by a loaded aperture. For other shapes of apertures, it can be shown that:

$$\frac{f_\delta}{f_{cs}} = C.\frac{D}{e} \tag{25}$$

with $1<C<2$. This means that as far as $D>e$, small holes in closed volumes will always dominate the skin effect through materials and will allow scattering of H fields in the volumes.

Geometry	Sphere of radius α	Cylinder of radius α	Circular aperture of radius α
Cut-off frequency	$f_m = \frac{3}{2\pi}\frac{Z_{s0}}{\mu_0\alpha}$	$f_m = \frac{3}{\pi}\frac{Z_{s0}}{\mu_0\alpha}$	$f_m = \frac{3}{8}\frac{Z_{s0}}{\mu_0\alpha}$

Table 4: Magnetic cut-off frequencies for different geometries with the a Z_{s0} surface impedance

Influence of contacts

The previous analysis of loaded apertures supposed a perfect contact of the aperture material with the structure. However, this contact is not always perfect. Figure 9-a shows a calculation of the effect of a non-uniform connection of a CFC panel on a square aperture (only two contacts between the two sides of the apertures) and a uniform connection perfect peripheral contact. This calculation has been made with Onera's EFIE computer tool. Figure 9-b shows several measurements of the shielding effectiveness of a panel in a TEM cell when the connection is progressively improved from badly connected (C9) to perfectly connected (C4). The effect of an imperfect connection clearly limits the shielding effectiveness.

It can also be shown that, even if uniform, the contact resistance of a lossy panel on an aperture will modify the f_m (19) and f_e (21) frequencies (f_m increases which reduces the shielding effectiveness).

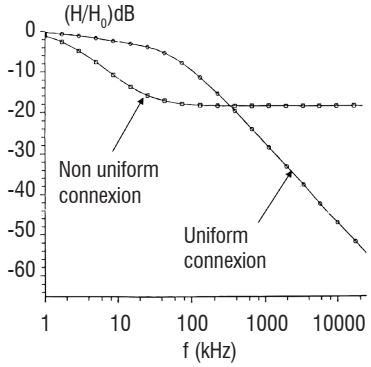

a) Magnetic field shielding effectiveness calculation

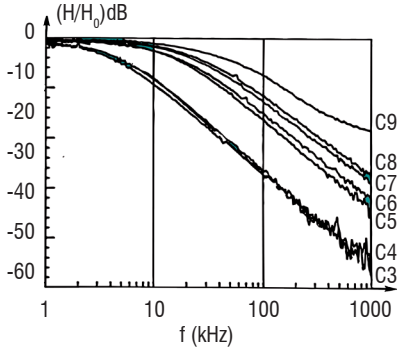

b) Magnetic field shielding effectiveness measurements

Figure 9 - Magnetic shielding effect for different types of connections of materials on an aperture (from [8])

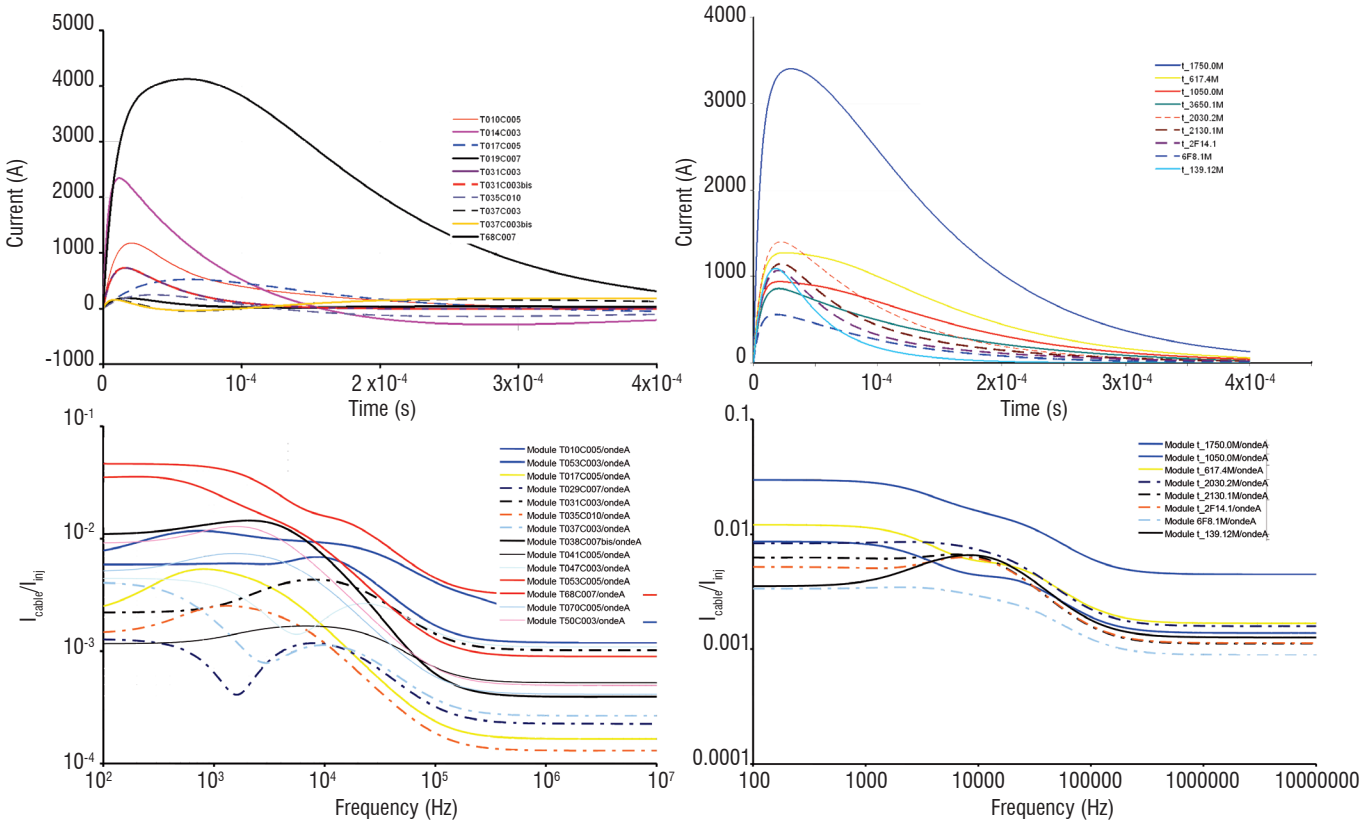

a) NH90 rotorcraft

b) Rafale fighter aircraft

Figure 10 - Low impedance cable currents on two AC/RC (time domain) and frequency spectrum of the Icable/Iinjected transfer function

Indirect lightning EM effects at system level

As far as system level is concerned, the emphasis must be put on cables, since cables are the major vectors of communication of electric and electronic equipment. When indirect lightning occurs on an AC/RC, cables behave as sensors, which capture some portion of the injected current and are thereby likely to transport currents that may be understood as useful electrical signals by electronic equipment. This is why, in this section, we try to analyze typical signatures of cables and we try to introduce main types of protection techniques, either at the level of cables or at the level of equipment inputs.

Typical responses of cables on AC/RC

EM coupling on cables is a particular case of the conduction effect. Figure 10 gives several examples of currents measured on low-impedance cables of the NH90 rotorcraft and the Rafale Fighter Aircraft for an A lightning waveform injected on the two AC/RC [32] in a coaxial-return test configuration [17], [18], [15]. The time domain and frequency spectrum responses of both AC/RC are very similar. The time domain responses show a distribution of maximums ranging between 3 and 4 kA and average maximums of about 1 kA. Almost all frequency spectrums of the Icable/Iinjected transfer function show a first low-pass filter cut-off frequency and most of the time a high frequency stabilized to a constant value.

Cables inside a cylinder

In order to explain the behaviors observed on AC/RC, we will first use a simple 2D model in which the 2D sections can be approached by a set of parallel wires supposed to be short-circuited at their ends. The box 2 shows a 2D invariant geometry of a plane approximated with 3 wires. The model allows the derivation of analytical formulas and shows the current redistribution trend. Such approximations can be generalized to more complex shapes and the formalism can be applied to all types of invariant 2D sections. This is an easy model to estimate the current redistribution for complex shapes and particularly the influence of cables, but this is also an efficient model to explain measurements. In such a model, low impedance cables are also described as thin wires short-circuited to the structure surface.

For the demonstration, let us first consider a 2 m-diameter cylinder (0.53 mΩ/m), with two 6mm-diameter inner wires (60 mΩ/m), one in the center and one close to the surface (10 cm) (figure 11-a). Figure 11-b gives the wire cross-section model of the cylinder with 80 elementary wires.

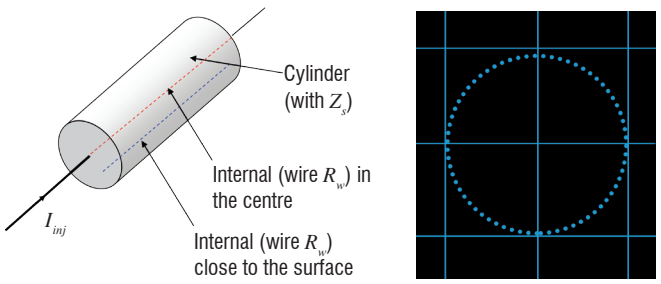

a) One wire in the center and one wire close to the surface

b) 2D wire model of the cylinder (the two inner wires are not represented)

Figure 11 - Cylinder with two inner wires

Figure 12 presents the frequency response of the two wires inside the cylinder. The Icable/Iinjected transfer function presents the same low frequency plateau and a quite similar cut-off frequency. It can be shown that the wire response transfer function (Iwire/Iinj) obeys the following low-pass filter law which gives a good approximation of the real responses observed on AC/RC (figure 10):

$$\frac{I_{wire}}{I_{inj}} == \frac{R_{structure}}{R_{\text{int}}}\left(\frac{1}{1+j\dfrac{f}{f_c}}\right) \quad (26)$$

with

$$f_c = \frac{R_{\text{int}}}{2\pi L_{\text{int}}} \quad (27)$$

where:

$R_{\text{int}} = R_{structure} + R_{wire}$ (transmission line resistance of the wire) (28)

and

L_{int}: transmission line inductance of the wire [31].

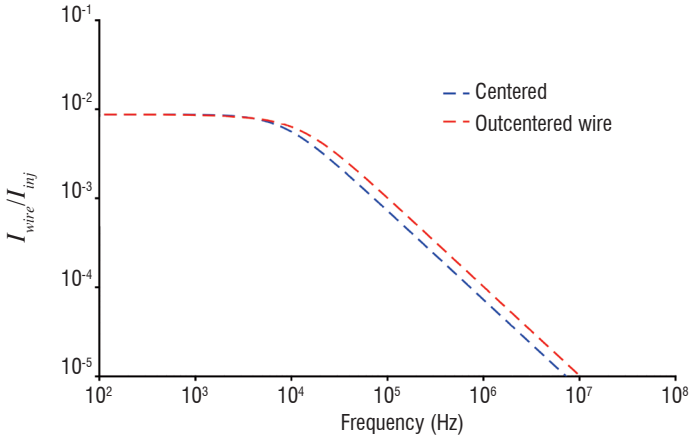

Figure 12 - Cylinder inner wire I_{wire}/I_{inj} transfer function

Cables inside and outside a realistic structure

Let us now consider a more complex 2D cross-section with angles (figure 13). This cross-section geometry is that of a NH90 helicopter [32]. In this case, unlike in the cylinder case, the redistribution effect may occur on the outer surface and has a significant effect on the cable responses, either inside or outside the structure surface. We observe that the inner wire responses all display a curve that is quite similar to a

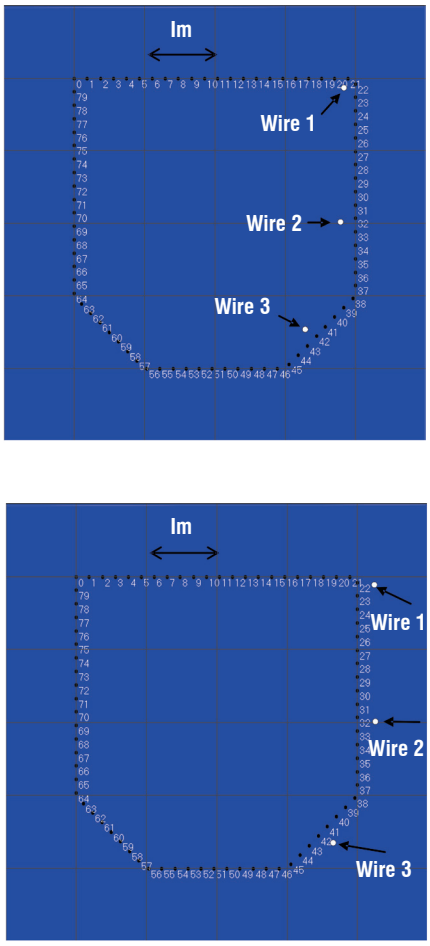

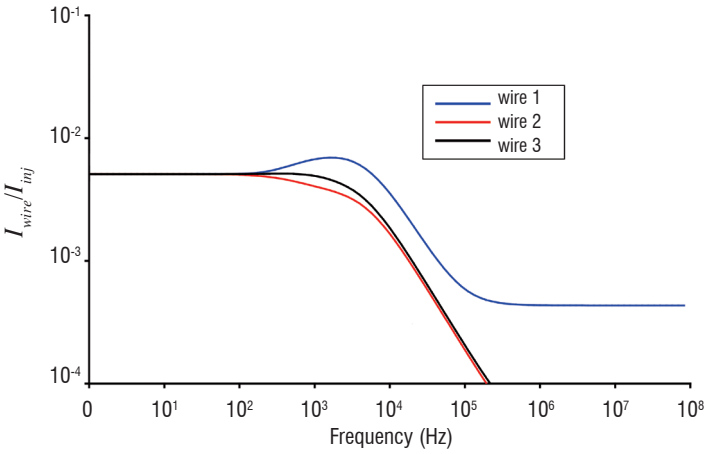

Inner cable response

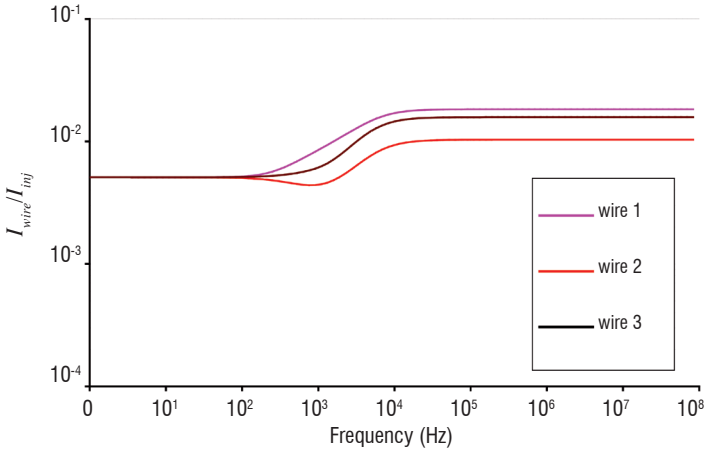

Outer cable response

Figure 13 - Realistic structure inner and outer cable I_{wire}/I_{inj} transfer functions

Box 4 - Thevenin equivalent generator on a cable due to an indirect lightning current injection

Let us consider the electric circuit represented in figure B4-1. In this figure, the ground reference surface is approximated by a single conductor on which a current I_{inj} is injected. Over this ground reference, we consider a cable, short–circuited at one end and in open-circuit at the other end. The cable over the ground conductor constitutes a transmission line characterized by:

- a resistance: $R_{\text{int}}=R_{cable+Rstructure}$
- an inductance: $L_{\text{int}}=L_{structure}+L_{cable}-2M$, where:
  - $L_{structure}$ and L_{cable} are the inductances of the structure and the cable respectively
  - M is the mutual inductance between the ground and the cable conductors.

Figure B4-1a represents the equivalent Thevenin V_{Th} model that must be evaluated.

The measurement of the open-circuit voltage allows the determination of the equivalent Thevenin generator, V_{Th}. The first contributor is due to the so-called "common-mode" voltage developed in the ground, V_{mc}. Since there is no current developed in the cable ($I_{cable}=0$), this common mode voltage entirely appears at the level of V_{oc} (figure B4-1b). The second contributor is due to the flux of the magnetic field in the loop formed by the structure and the cable. This flux is obtained from the mutual inductance between the ground and the cable conductors and the current flowing in the ground. Note that this contribution ends up with a derivative of the injected current (figure B4-1c).

At the end, we can write:

$$V_{Th}=\left(R_{structure}+j\omega M\frac{d}{dt}\right)I_{inj} \tag{29}$$

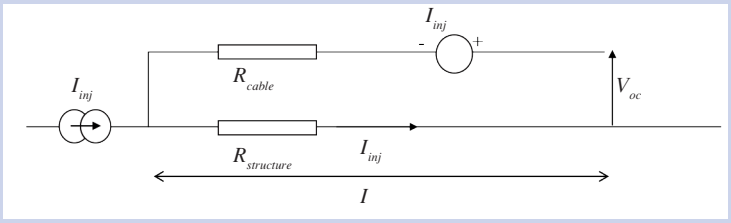

a) Problem to solve

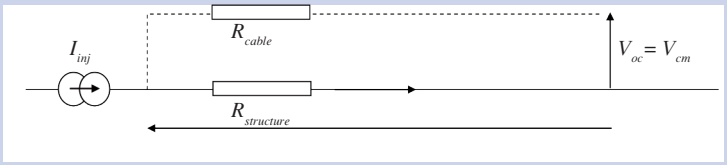

b) Common mode voltage coupling

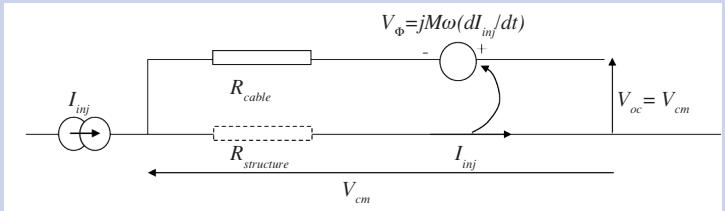

c) Magnetic flux coupling

Figure B4-1- Thevenin generator on an open circuit wire in the case of a lightning injection

low-pass filter, but the cut-off frequency depends on the position of the cables. Particularly, we note that the cable in the upper right corner presents an overshoot before the cut-off frequency. Note that the constant level observed for this wire at high frequency is due to the discretization of the surface in thin wires. With more wires, this level would get lower. In reality, for a full surface, this constant value does not exist and the plot continues on its 20dB/decade decaying slope. Such behaviors are very similar to those observed for the determination of transfer impedance (Z_t) of shielded cables with no circular shields [33].

When the wire is outside the structure, the behavior is quite different since it becomes more like a high pass filter characterized by the fact that the current accumulates in the most exterior parts of the structure, which become the external wires (the flat level at high frequency is due to the thin-wire discretization). Note also here the undershooting phenomenon, which is now occurring on wires parallel to flat parts of the geometry.

Main characteristics of cable responses on AC/RC

Lightning indirect effect coupling on cables is due to the conjunction of two voltage sources (see box 4):

• a common mode coupling, which is due to the development of an electric potential difference on the structure;

• the magnetic field coupling due the magnetic flux inside the loop made by the cable.

For a given injected current, the significant cable currents are scaled by the resistances existing between the connection points of the cables.

In [32] a large investigation has been carried out on two databases of low-impedance cable responses in the Rafale fighter aircraft and in the NH90 helicopter, subjected to an A-lightning waveform injection. This analysis resulted in very significant lessons available for those two types of air vehicles:

• The current on cables is mainly on branches oriented in the direction of the current on the structure. Therefore, if the current is injected longitudinally as for most coaxial-return configurations, the current along branches that are orthogonal to this main direction is low. Along these orthogonal branches, the response is mainly derivative, which means that the coupling is dominated by the coupling due to the scattered field (see Box 4). Such derivative waveforms are also observed for exposed cables, in open areas such as cockpits. Actually, the injection and output points define a transverse variation of the electric potential difference between those two points, which defines at the same time the cable branches supporting the maximum current;

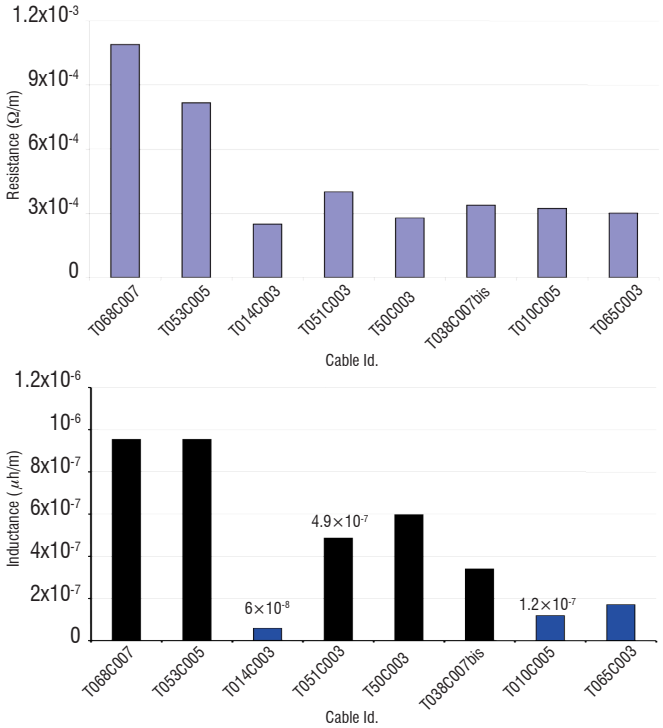

Figure 14 - Low per-unit-length resistance and inductance of low-impedance cables on the NH90 helicopter

• The resistance of the structure can be approximated as a function of the connection points on the aircraft/rotorcraft structure: knowing the height of the cables with respect to the structure, the transmission line inductance L_{int} can be estimated and the analysis of the cut-off frequency of the I_{cable}/I_{inj} transfer function as in (26) thereby allows the identification of the R_{int} (internal resistance) parameter of the low impedance cables (or the parts of the harnesses longitudinal to the current injection into the structure). As an example, this distribution of resistances in Ω/m is reported in figure 14, with a larger distribution for resistances of about 0.3 mΩ/m. From this, if we are able estimate the per-unit-length resistance of the cable shields (an average of 15 mΩ/m is a reasonable approximation), it is possible to estimate the resistance of the structure as a function of the position along the longitudinal current injection axis (figure 15). In this figure, the various straight lines correspond to various longitudinal cable parts having been used to determine the resistance of the rotorcraft between two connection points. The starting coordinate and the end coordinate of those straight lines are referred to a longitudinal position between the two ends of the helicopter in the coaxial return. Of course, the shorter the line, the smaller the impedance. From this figure, looking at the blue and black line, we have an indication that the total resistance of the structure varies between some mΩ and a few tens of mΩ.

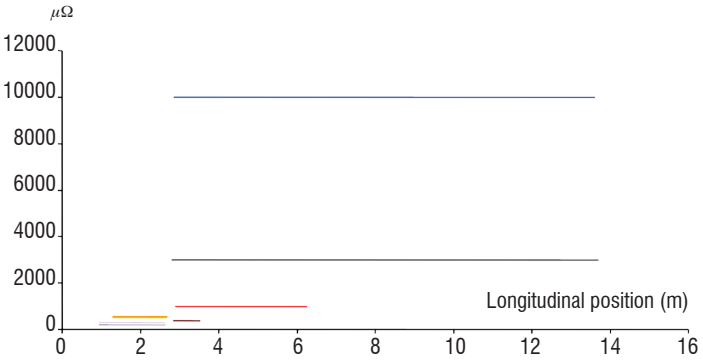

Figure 15 - Resistance of the structure on the NH90 helicopter (each test-line corresponds to a point-to-point longitudinal cable-harness branch)

Justification of the linearity hypothesis

So far, we have made the approximation of linearity of the entire phenomenon. However, lightning is a high level environment constraint and it is important to consider possible non-linear effects. For example, it is known that at the material level, the application of high intensity currents changes the electrical characteristics of the materials, especially their electric conductivity. This is also true for the contact resistances at the level of panel junctions, whose conductivity may also improve when submitted to high level currents. Thus, even if this phenomenon is real, the control of non-linear effects occurring over an entire system becomes very complicated. In the following section, we try to assess to which level the linear approximation remains conservative, in terms of the current level specified at the level of equipment inputs.

Figure 16 shows different Iwire/Iinj transfer functions obtained by different techniques on the same cable in the same system:

• with low-level current injections (with a CW measurement directly made in the frequency domain with a network analyzer and with a low level A waveform injection). This first set of waveforms gives the same transfer functions and testifies that the injected current did not produce any non-linear effects;

• with two medium-level waveforms (some 10 kA) with a high dI/dt derivative (similar to a H waveform). These transfer functions are different from each other, with the previous reference levels, with no non-linear effects;

• with a high level A waveform injection. This transfer function gives another transfer function with the lowest level.

These plots show that the higher the injected current, the lower the transfer function at cable level. This also means that the higher the injected current, the better the shielding brought by the system surface is. This means that the non-linear effects allow better circulation of the currents (less overall resistance).

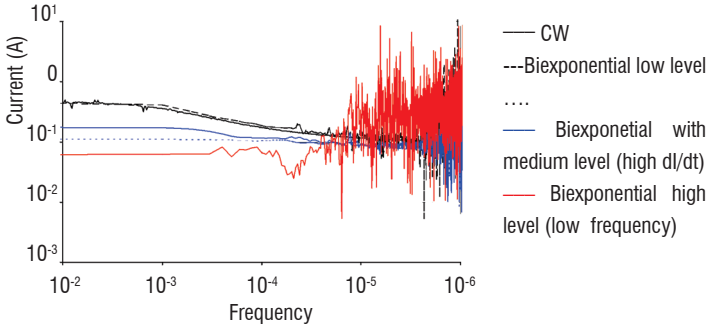

Figure 16 - Measured I_{wire}/I_{inj} transfer functions

In Figure 17, we show the effect of such transfer functions on the time-domain waveforms. Figure 17-a displays two frequency responses for currents measured directly in the frequency domain and obtained on two different cables, as well as the Fourier transform of the injected current (similar to an H waveform). Cable 1 is an open cable, not shielded, whereas cable 2 is a cable inside a shielded cable bundle. Figure 17-b and figure 17-c show the time-domain responses of the two-cables obtained from the transfer functions, compared to the measurement of the current on these cables directly measured in the time domain. Figure 17-b shows that the calculated current for cable 1 must be multiplied by a factor 1.5, in order to find the measured time domain waveform again. Figure 17-c shows that the average level has been well calculated, but the waveform is quite different from the measured level, which clearly shows a waveform signature that we may attribute to a non-linear effect having occurred at the level of the cable or more likely, of its connector.

As a conclusion, non-linear effects clearly occur during indirect lightning current injections, but they are difficult to control. Nevertheless, linear approximation of the phenomenon gives a good estimation for the specification of currents induced at the level of equipment inputs.

System level indirect lightning protection

A straightforward but false idea for lightning environments would be to use installation rules such as to locate sensitive equipment in EM "clean" zones, but this concept cannot work because, as a low frequency phenomenon, lightning conduction is very effective over long distances, especially along cables. Therefore, cables running in EM exposed zones can pick up some interference and drive it up to the level of an equipment box located in a non-exposed zone. Second, cables are organized in cable bundles, which group them all together; clean cables can be spoiled by "dirty" cables. Nevertheless, each aircraft manufacturer applies segregation and installation rules between cable bundles which allow all types of EMC cross-coupling related

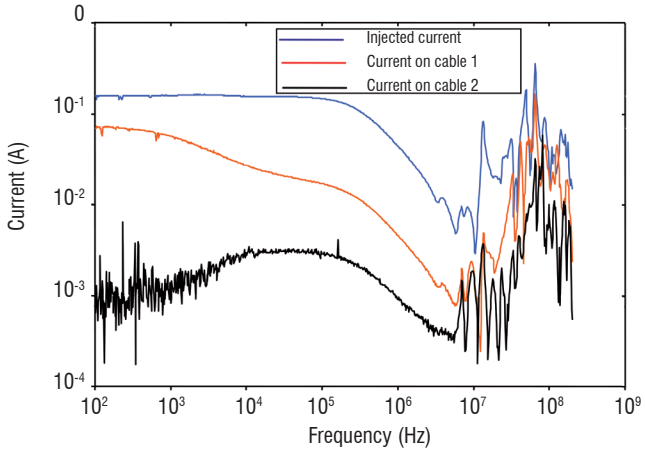

a - Measured transfer functions

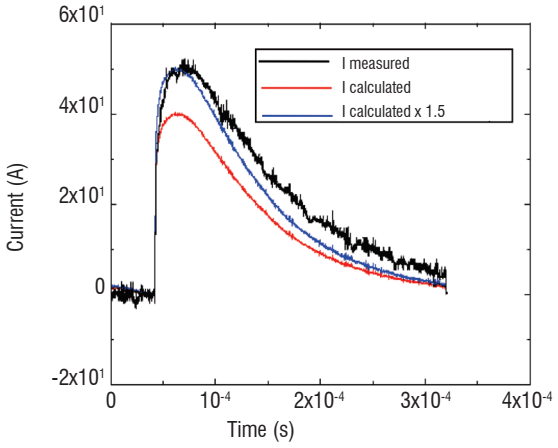

b - Time domain waveforms for cable 1

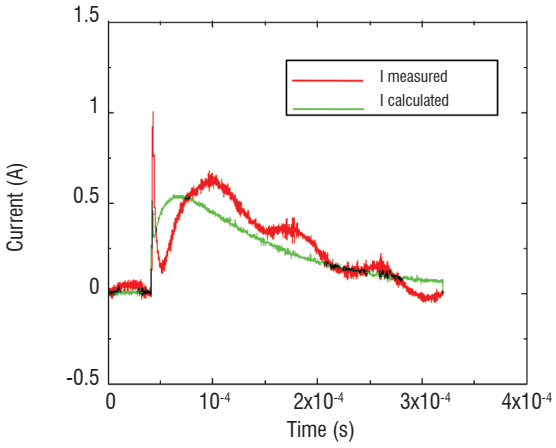

c- Time domain waveforms for cable 2

Figure 17 - I_{wire}/I_{inj} transfer functions generated from measured currents on systems

problems to be sustained. Solutions at use are: separation of cable-bundles with a standardized distance, routes of cable-bundles at specific distances from the mechanical ground.

System level protection against indirect lightning can be seen at three levels: structure level, cable-level and equipment level. As far as system protection against any type of EM effect is concerned, the rule is generally to take advantage as much as possible of the protection that can be naturally provided by the geometry of the structure and the installation of the electric and electronic system. This is why this natural protection is called "passive" protection; it may concern the structure and the cables. Such protection consists in optimizing the shielding effect by maximizing the current that is supposed to circulate on the shields. Such concepts are the ones considered in the theory of EM topology [34], in which design rules are based on the concepts of generalized shields. In this approach, the main rule is that the interacting currents must be concentrated as much as possible on the outside of the structure, using several embedded layers of shields. Even though this design approach cannot be applied as such for indirect lightning, the approach provides very useful guidance rules for designers. Indeed, the more the EM design is controlled and the more the control of possible EM problems will be in the future life of the system.

When all passive shielding protection measures have been applied on the installation, the only solution to improve the protection is to apply the protection directly at the level of the equipment. For this, active non-linear devices are applied on each critical pin, in order to short-circuit unwanted current amplitude to the ground in the event of critical interference. In this paper, oriented on EM aspects and related methods, we will only consider passive protection.

Topology-based protection

Material and structure protection constitutes the first EM shielding volume according to EM topology decomposition. From a practical point of view, the idea is to help the structure act as the best shield possible. For this, depending on the mechanical and budget constraint, several parameters can be optimized for indirect lightning:

- the shape of the structure: we have seen that the closer a cross-section geometry is to a cylinder, the better the current is equally distributed around it. This is the typical case of the fuselage geometry. On the contrary, a current on flat shapes increases the possibility of having current redistribution in the corners and thereby increasing field penetration at this point. From a practical point of view, it is not realistic to think of modifying a shape to make it a cylinder, but it may be clever to take advantage of a cylinder shape and not break its natural symmetry or make its electrical properties dissymmetrical;
- The global conductivity of the structure, in order to drive as much current as possible on this structure. Aircraft manufacturers must comply with specific requirements for the DC resistance of the structure. We have seen that direct lightning metallic grid protections applied on carbon composite materials had a significant impact on the improvement of the Z_s surface impedance and, consequently, of its equivalent electric conductivity. Since the objective of such protections is to facilitate the circulation of the current injected at the lightning striking point, this technique is also well suited to improve the global EM shielding efficiency of the structure, provided that the continuity of the currents is maintained. This typically means that the electric continuity between the panels must be as good as possible. Especially at the design and maintenance phases, efforts must be directed towards achieving the uniformity of the contact, rather than the improvement of the local contacts. Each diversion of a current line or its concentration along a given path is likely to generate EM scattering (see § EM scattering effect);
- In addition to this EM effect, the bad contact or, worse, the isolation between two structural parts supposed to be on the normal evacuation path of the current may lead to an increase in the potential difference between those two parts and may create an electric breakdown between them, as was already mentioned in § Indirect lightning EM model related issues;
- The minimization of the apertures: while efforts have been directed at the geometrical shape and the global conductivity, global EM optimization consists in minimizing the EM scattering effect at openings, such as cabin windows or cockpit canopy: this is done by decreasing their number and their size. If possible (that is to say, if it does not alter visibility), a solution is to use metallic grids, provided that this grid remains in good contact with the structure all around the aperture. The cells of the grid act as small apertures, for which the combined global attenuation is larger than the attenuation of the free aperture [25].

Bounding and Grounding

Bounding and grounding techniques are techniques generally required for electric safety. However, they must be applied properly, in order to be compatible with EM external threats, especially threats such as indirect lightning. Let us also recall that such techniques are effective at low frequencies only. This is why techniques for bounding and grounding always require a short connection and low impedance connections, which leads to the use of large-section conductors or braids.

Bounding consists in connecting all of the conducting parts together, in order to maintain the same electric potential, at least at DC. This action prevents electric breakdown from developing between equipment parts and cables.

Grounding consists in connecting a conducting part to the "ground". For indirect lightning and for all EM threats, the ground to be considered is the "mechanical ground" constituted by the structure surface itself, since this structure is the main contributor to the dissipation of the current.

The development of non-metallic aircraft, such as full composite carbon aircraft, raises the question of the efficiency of grounding and bounding and its compatibility with electric safety rules. Such a concern is very similar to the problem encountered in ground installations (see [35]).

The absence of a structure surface that is conducting enough to be considered as a good mechanical ground makes it necessary to recreate this ground reference by introducing a grounding network, which partly cancels the weight reduction advantage claimed by the use of carbon composite materials. Different techniques may be proposed, from bus-bars to metallic tubes, for building this network. The first one offers simplicity of maintenance on cables and electronic equipment, which is not the case for the second one. However, the second provides efficient cable shielding at the same time as the ground reference. The use of raceways could be a good compromise for the tubes and they may be used in combined configurations with bus-bars.

Box 5 - Transfer impedance of a cable-shield

Even if the shield connection is made at both ends, this does not mean that the shielding attenuation is perfect. As for material, the shield possesses an electrical conductivity, which therefore allows penetration of the magnetic field. In the same way as we have said that materials could be characterized by a Z_s surface impedance quantity, the shielding property of a cable-shield can be characterized with a quantity, homologous to a per-unit-length (p.u.l.) impedance $Z_{t,}$ called the transfer impedance.

Provided that the shield is well connected at both of its ends, the coupling model on the inner wire $V_s(z)$ is obtained by applying a distributed voltage generator of the type:

$$V_s(z)=Z_t.I_s(z) \tag{30}$$

where $I_s(z)$ is the distributed current on the shield and z is the position along the cable.

From a modeling point of view, the Z_t concept therefore allows the decomposition of the problem of EM coupling evaluation along the cable into two independent problems:

- the evaluation of the current on the shield, Is
- the evaluation of the response of the inner-wires. The interest in this part is that the inner-wire geometry is fully appropriate for the application of Multiconductor Cable models, in which the shield is the reference of the transmission lines.

Note that as there is a Z_t parameter relating the shield current to the inner equivalent voltage source; there is also a transfer admittance called Y_t that relates the shield voltage to an inner equivalent current source, due to small holes existing in braided shields, for example (see § Loaded small apertures).

Note also that the Z_t parameter is an integral part of multiconductor p.u.l. electrical impedance matrices, since it describes the relation between the inner and outer transmission line when this model is applicable for the shield with respect to its reference. This parameter therefore plays a reciprocal role; an interference signal on the inner wires induces current on the outer surface of the shield [36].

At DC, it can be shown that the Z_t is real and is equal to a quantity called p.u.l. "transfer resistance", R_t, itself equal to the p.u.l. resistance of the shield. Then, when the frequency increases, because of the limitation of the current on the outer surface of the shield, the transfer impedance improves with a damping to zero. If the braid were a full thick cylinder, such damping would continue with the increasing frequencies. However, because overshields are made of metallic braids, the braids leave a multitude of small holes that will act as small apertures (see § Free small apertures) and let the magnetic field penetrate. Because this scattering effect is a derivative phenomenon in the time domain, the transfer impedance can be characterized by a p.u.l. quantity homologous to an inductance and called "transfer, inductance", L_t. If this scattering effect arises before the skin effect, the damping effect, also called Schelkunoff effect, does not show up [37]. Without this effect, the transfer impedance can be simplified under the form:

$$Z_t(\omega) = R_t + jL_t\omega \tag{31}$$

As far as indirect lightning is concerned, the scattering by those small holes is not relevant. However, it is relevant for higher frequencies, such as HIRF frequencies, and we must consider that cable overshields are generally installed for a wide frequency band protection.

Figure B5-1 shows the typical variation of a cable-shield transfer impedance, with and without a Shelkunoff effect.

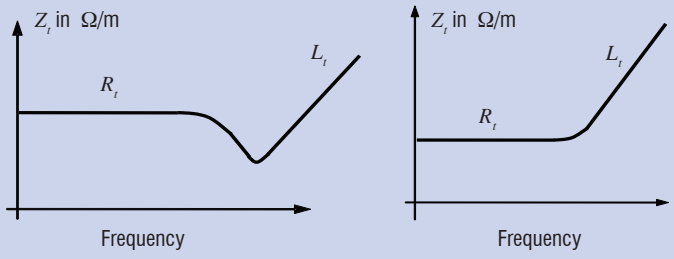

Figure B5-1 -Typical frequency variations of the transfer impedance of a shielded cable

The transfer impedance usually depends on the position of the wire in the cable-shield. In order to illustrate this point, we have shown in figure B5-2 the variation of the field inside a very specific shield design used to drive cables from the technical premises of a ship radar to the ground, in a so-called "transparent mast" [33]. This shield has a rectangle cross-shape on the left-hand side and a circular shape on the right-hand side. The inside walls are included, in order to separate volumes. In figure B5-2 the penetration of the H field is indicated with a color code. Square meshes indicate the relative amplitude only but the example allows the current redistribution effect happening also at the scale of this shield to be put to the fore. At a low frequency (10 kHz), the penetration of the shield is mainly due to Rt and is therefore homogeneous. When the frequency increases (1 MHz), due to L_t, the magnetic field begins to lower in the middle but increases along the walls, in the corners and in the middle of the circular shape. In addition, the field is quite important along the vertical wall in the half right-hand side circular volume. This behavior is accentuated at 10 MHz, for which the field significantly decreases in the middle of the straight surfaces. At very high frequencies, the internal field vanishes everywhere inside the shield. Figure B5-3 summarizes this frequency variation of Z_t at several test-points. All of the plots clearly show the R_t constant value and the start of the 20dB/decade L_t slope, but several overshoots corresponding to test points in the corners or in the middle of the half-circular surface are also displayed, as observed in Figure 13.

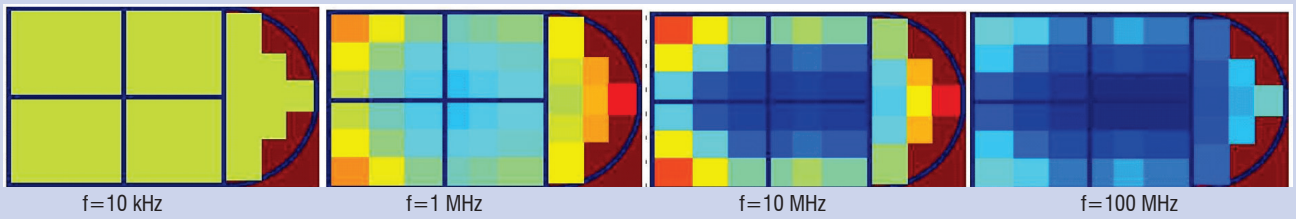

Figure B5 - 2 - Frequency variation map of the field penetration for a specific shape shield (levels are masked intentionally) – the scale color varies from dark-blue – light blue – green – orange –red. Brown stands for "not-defined"

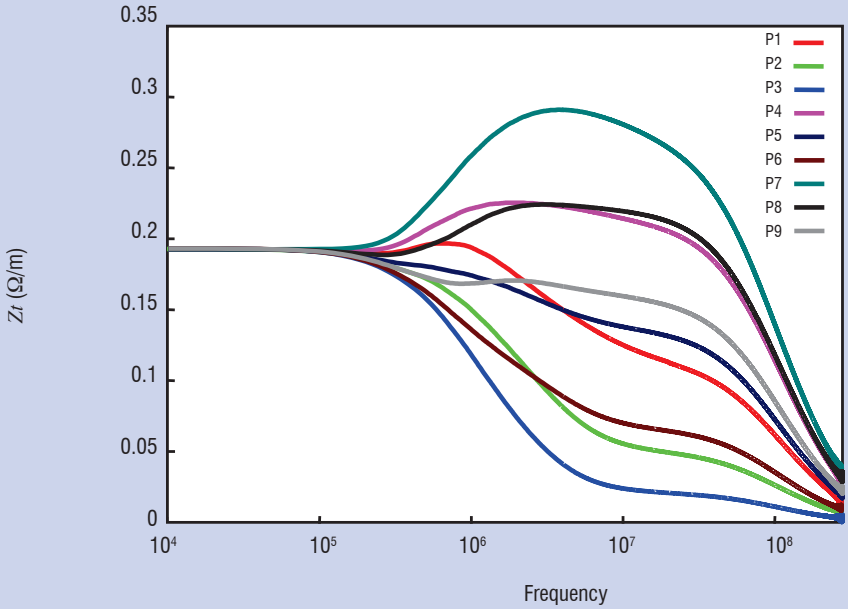

Figure B5 - 3 - Frequency variation of Z_t at various test points (P1 to P9) inside the specific shape shield in figure B5-2 (the location of the test-points is intentionally masked in Figure B5-2)

Protection with shielded cables

Cable shields have three main functions for signal cables and electrical wires: 1 – For mechanical protection, 2 – for optimizing the propagation of the signals (in order to transmit high frequency signals, for example), 3 – for providing an EM protection and making the mechanical shield become an EM shield. Here, we focus on the third function. The EM shields take the form of metallic braids that uniformly surround the cable bundles (the braid allows the overall bundle flexibility to be preserved, compared to a rigid tube). Such shields are called overshields (they may overshield cables located inside).

We have seen that current injection in the aircraft/rotorcraft structure generates equivalent common mode and mutual inductance sources in cables. In order to reduce the amplitude of those sources, the idea is interpose a shield that will act as a second shielding level after the structure shield, in terms of EM topology. However, in order to obtain this shielding level, we must allow the current to flow on this metallic conductor. This thereby requires that the shield be well connected to the mechanical ground at both of its ends in order to provide both the magnetic and the electric shielding effects (by the way, the electric shielding effect can be obtained with only one connection at one end of the shield).

Now comes the question of how to make the connection to the ground. As said for the equipment, the connection must be as short as possible, in order to lower the dynamic impedance. For the indirect lightning effect, a simple wire or braid connection is sufficient.

Nevertheless, the installation must avoid the following mistakes regularly encountered on systems:

• do not use long braids which will increase the inductance and may lead to an increase of the global shield impedance;

• if long braids must be used, do not make loops by winding them on themselves and therefore developing an "efficient" magnetic collector, likely to couple to the wiring;

• do not make the connection to a pin of the equipment chassis connector.

If the shield requires an EM protection function at higher frequencies for other EM threats (such as HIRF for example) and if it is affordable, the installation should use a 360° circular connection of the shield on the equipment connector chassis. This will avoid any inductive connection effect.

Finally, installation should be done taking the opportunity of connecting the cable overshield to the ground as often as possible. On the one hand, for regular use, this avoids resonance of the cable overshield, but this is not of real concern for indirect lightning. On the other hand, if this connection is made for each crossing of walls, this technique allows the shield induced-currents to be confined in specific zones, without transmitting them in undesired zones.

As a conclusion, we can propose the following good trade-off rules for the proper use of cable EM shields with respect to indirect lightning effects:

• always connect the cable shields at its ends at the level of the equipment;

• take advantage of intermediate connections to the ground, in order to enforce the effect of zone decoupling;

• use cables with a good resistance per unit length.

Remember also that a cable-shield that is not connected at both ends will not provide any magnetic shielding effect along the inner cables, whereas a single connection at one end provides only an electric shielding.

System level numerical simulation

As in every electrical engineering process, numerical simulation nowadays plays a major role [38], [39], [40]. The interest in using numerical simulation can be seen at two levels:

• for analyzing measurements. In this case, the simpler the model, the better the analysis. This is typically what has been shown in this article when 2D invariant models are used to understand EM coupling mechanisms on structures and cables,

• for predicting the constraints to be applied at equipment level on real systems. In this case, the model must be as precise as possible and must take into account the entire system. The trend is increasingly for the generation of such EM models to become part of industrial process for the design of the system and even the certification. Let us mention for example the significant part played by EM demonstration in the new version of ED107 for HIRF [41]. Let us also mention the HIRF-SE project, which is aimed at considering EM modeling as an integral part of the HIRF certification process [42].

In this section, we are interested in the second aspect of indirect effect modeling. Let us specify that in such cases, the objective can also be to help in the building of the experimental test program and to be able to extrapolate the test results to configurations that cannot be tested.

Indirect lightning EM modeling specificities

The numerical tools concerned by these types of heavy EM modeling processes are so-called "3D computer tools". These tools are based on a discretized resolution of Maxwell's equations [43], either in their differential form or in their integral form, applied on a discretized model of the geometry on which EM and electric characteristics are applied (the mesh). The modeling process is thereby divided into 3 usual steps:

• the generation of the mesh (geometrical and electrical model). This task is accomplished by means of tools called meshers;

- the availability of the geometrical model comes from CAD models. Two main types of geometrical models are generally considered: surface and volume meshes.

◆ on the one hand, most commonly used surface meshes generally consider only thin surfaces, which is a quite reasonable approximation for indirect lightning but they may suffer limitations if lossy volume materials must be considered. The advantage of such techniques is the good conformity of the generated meshes. However, while the generation of the outer surface is generally not a key problem, the generation of a precise model of the interior involving all of the constitutive parts is a real problem

◆ on the other hand, the most commonly used meshes are structured meshes with models discretized in small cubes. The technique for generating such geometrical models is based on the interception of a Cartesian grid with the real geometry description (CAD model). The conformity to the real shapes is therefore limited to the cubic approximation. However, small cells of about 5 to 10 cm are generally sufficient to obtain a good approximation of the external surface for indirect lightning concerns (Figure 25-a). In addition, this cubic representation becomes a real advantage compared to conformal meshes as soon as the model of the interior geometry is concerned.

- the availability of the electrical and EM models generally comes from databases (databases of materials, cable database). As seen before, Zs material models are well suited for thin surfaces; lossy materials are sufficient to describe lossy contacts. When EM scattering through holes or seams is concerned, macro-models of small apertures, as seen in § "Free small apertures", are appropriate.

- as far as cable models are concerned, models of thin wires are used; they are based on an approximation of a homogeneous current in the cross-section and they usually require to be much smaller than the cell-size. Multiconductor Transmission Line Network (MTLN) models [44], [45] can be interesting for calculating current and voltage levels precisely on specific wires or pin-connector ends. However, for indirect lightning, it is sometimes difficult to include the common mode resistance in the MTL models for the electrical parameters, because the return of the current depends on the 3D geometry (for higher frequency threats, the current mostly returns under the cables). For this reason, the application of field-to-MTL approaches, which allow coupling 3D solvers and MTLN solvers, is not fully appropriate or requires at least precautions [31], [46], [47]. From a practical point of view, coupling with 3D solvers is therefore mainly possible with shielded cables. The 3D solver calculates the current response on meshed equivalent wires of the cable-shields and MTLN models calculate the responses of wires inside the shield, using its Z_t transfer impedance (see § "Protection with shielded cables").

In Figure 18, because of the small cell-size, it has been decided to mesh the bundles as rectangular cross-sections along the Cartesian mesh, in order to better approach the real size of the cable-bundles and in particular to better approach their self-inductance. Considering the overall complexity of the problem, it is not certain that a thin wire approximation would not have given similar results.

• the resolution of Maxwell's equations for the geometrical and electrical model. The technique of resolution generally depends on the type of mesh, since the geometrical decomposition conditions the type of Maxwell's discretization. Generally, for various reasons, such as stability of numerical schemes, volume techniques are solved in time domain; the Finite Difference Time Domain technique is one of the most favored approaches for the many advantages that it provides [43]. Surface techniques are solved in the frequency domain with resolutions of the Moment Method type. Volume techniques require absorbing boundary conditions for limiting the calculation volumes, such as ML, PMLs [48], [49]: this also allows infinite wires to be considered to simulate the lightning injection channel. Surface techniques do not require such conditions, but they suffer the fact that it is impossible to consider infinitely long wires.

• the post-processing covers the usual task of displaying results in one, two or three dimensions with a specific objective to be able to handle large sets of data, especially in 2D and 3D (figure 18-b). Another specificity is the extrapolation of time domain signals to zero for time domain calculations. Indeed, due to the long calculation time, 3D calculations are generally stopped sometime after the maximum of the waveform has passed. This return to the zero signal is required, because it is the only way to determine the action integral or the frequency content at the zero frequency. Several techniques can be applied: we can mention the techniques based on autoregressive techniques (such as Prony techniques) [51] or on the decomposition of sums of biexponetial waveforms, such as the Levenberg-Marquardt technique available in the XMGRACE freeware tool [52].

Indirect lightning EM model related issues

The challenges for building and solving indirect lightning on a 3D discretized model can be synthesized as follows:

• the cleaning of the geometry, which consists in removing all parts that do no significantly participate in the EM response and the morphing of the cells, in order to correct approximations generated by the cell discretization (correction of the contacts between parts, especially).

• the correct evaluation of the contact resistances to be placed at junctions between mechanical parts. This type of information is quite difficult to obtain from a data base, because it is highly system-dependent (unlike the resistance of a cable or the characteristics of a material).

• the management of the size of the geometrical models. A usual requirement is to be able to consider the quasi-static approximation in each cell of the mesh, which commonly leads to an approximation of the type $\lambda/10$. Therefore, for indirect lightning, this condition should lead to cells of some meters only! Nevertheless, small cells are required in order to describe correctly the geometry and particularly the contacts or absence of contacts between zones or cables. For time domain resolution, stability criteria imply small time steps and lead to long resolution times. In addition, large meshes imply efficient hardware and software to display the views of the mesh, since the amount of data is generally huge (of tens of millions of cells).

• the availability of cable architecture in the CAD models. The wiring database must include at the same time the wiring topology and its constitution; unfortunately, such information is not always jointly available. In addition, the problem is to be able to run the cables (volume models or 3D models) in a consistent way. In figure 18-a, cables have been meshed in surface because they are shielded cable bundles whose radius is large compared to the cell size (0.5 cm). The difficulty is of course related to the constraints generated by the Cartesian grid. In box 2, an original and new technique of multiconductor

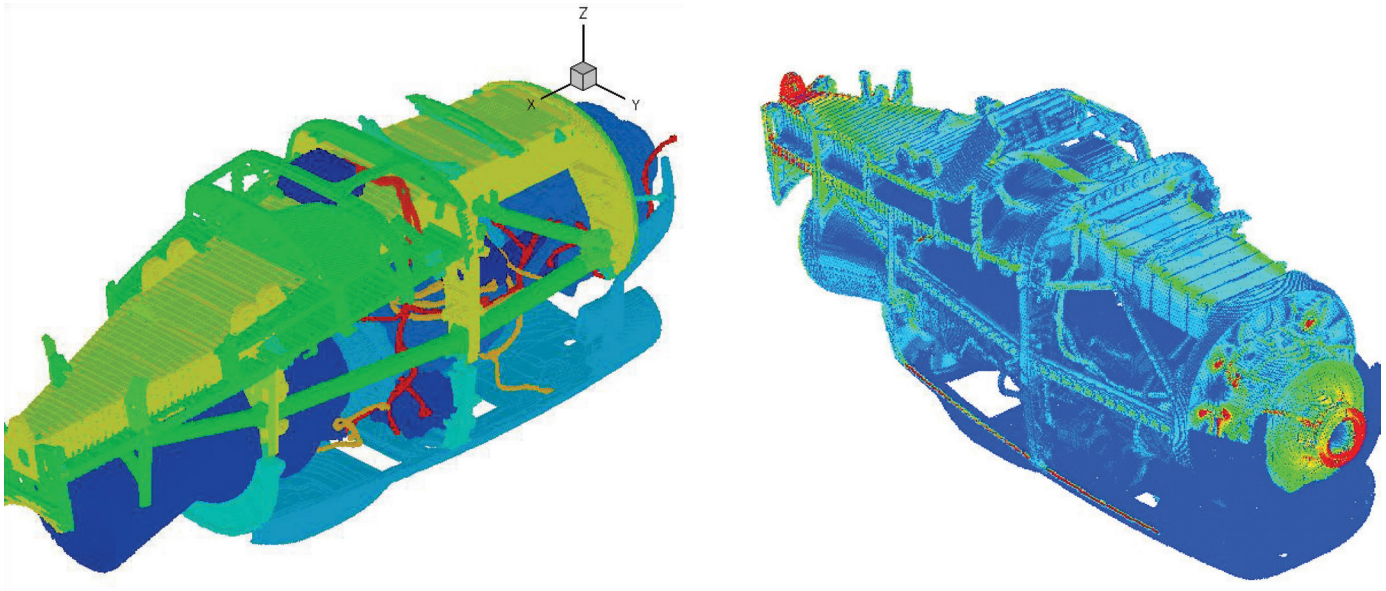

a) 3D FDTD model

b) Current distribution

Figure 18 - 3D FDTD model of the TP400 engine (from [50])- Courtesy of HISPANO-SUIZA

Box 6 - Modeling bent wires in a simulation of indirect lightning on the Falcon 7X aircraft

In [53] and [54] a very complete work is shown to describe how the methodology of indirect lightning modeling can be carried out at the level of an entire aircraft. This work, carried out within the framework of a cooperation between Dassault and Xlim in France, can be seen as an extension of several studies carried out within the framework of aircraft certification, such as the one described in [40] for the certification of the C 27J Italian aircraft. In Dassault's and Xlim's paper, the authors use an FDTD approach in [40] which gives further evidence of the robustness to carry-out extensive EM 3D calculation, as far as tackling the full complexity of an aircraft system is concerned. However, Dassault's and Xlim's authors go a step further by providing, at the same time, a solution to 3 main challenges which currently limit the application of FDTD techniques on such large problems:

Calculation of late times

As we have seen, it is essential to obtain the long times of the induced signals because they are required to have a good estimate of the action integrals and therefore of the induced energy. The French authors propose the combination of two techniques:

- the Matrix-Pencil method (MP) [55] developed by T-K. Sarkar to extrapolate long time signals using poles and residues decomposition techniques, based on the Singularity Expansion Technique (SEM)
- the Short Impulse to Large Impulse (SILI), which calculates the transfer function over a large frequency band in order to be able to determine the response of the system to any type of injected current waveform.

When these two techniques are applied for estimating current responses in cables, this technique allows the extrapolation of 50 μs responses to 1ms responses.

The positioning of cable models anywhere in the aircraft model

We have seen that realistic models of an aircraft system require the possibility of modeling a large set of cables. Of course, more and more CAD models provide cable route geometrical data, but the problem of describing it correctly in the meshed model remains. For this, the thin wire model [56] is a good approximation, but the model requires the route to follow the edges of the Cartesian grid, which results in having all of the meshed routes described in steps. In addition, the bad description of the routes is not the only limitation; the restriction of having wires along the edges implies merging some cable-links in unique equivalent cable models, which of course changes the electrical circuit followed by the flow of the current. This is why Dassault and XLIM have been working on the development of a thin bent wire model, which avoids those limitations and allows very realistic aircraft wiring systems to be obtained, as far as indirect lightning is concerned. This feature has been integrated into XLIM's FDTD 3D computer tool; wires can be placed anywhere in the FDTD Cartesian cells; several wires can even be placed in a given cell. It has been used for all of the cable results presented in [53] and [54] (figure B6-1).

The incertitude on cable-losses and end impedances

As regards indirect lightning, we have seen the relevance of two major factors:

- the common mode impedances, which depend on the material electrical characteristics and the connection impedances at junctions.
- the cable impedances. These depend on all of the elementary cables, which constitute the thin equivalent model of the cable-bundles.

Therefore, both parameters cannot be fully deterministic. [53] and [54]evaluate several designs of experiment methods to estimate extreme values of signals resulting from these uncontrolled parameters. One of the main lessons is that the Rechtschaffner method [57], based on simplified fractional plans, gives very satisfactory results compared to more exhaustive methods.

The main interest of this very complete work resides in its application to Dassault's F7X aircraft and its comparison to real measured signals, which provide a clear validation of the method for using it, for certification purposes. This is why, at the time of the publication of this article, this work may be presented as the most achieved state of the art of lightning indirect modeling at the entire aircraft level.

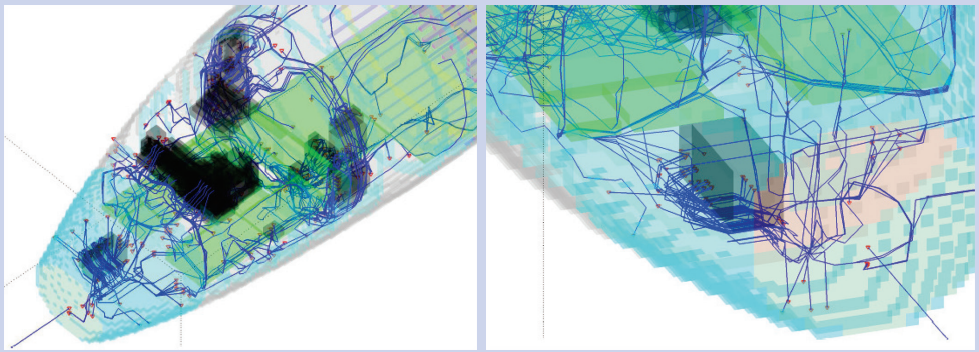

Figure B6 -1 - Details of Dassault's F7X wiring model inside the FDTD model (form [54]). Courtesy of Dassault

wires, not necessarily parallel to the Cartesian grid, has been used and opens a new field for describing the large density of cables in 3D interior geometry.

• identification of zones of electric breakdown. We have seen that it is difficult to control non-linear effects due to indirect lightning. In particular, electric breakdowns occurring between geometrical parts, especially junctions, are of particular importance. For this the determination of zones in which the electric field may be of the order of magnitude of electric breakdown in free space (typically 3 MV/m) is a very good indicator. Thus, the simulation of the electric breakdown with a thin wire with a specific resistive law may provide very good indicators in terms of design. Nevertheless, the prediction level is not achievable yet.

New trends

3D modeling is so far based on the resolution of Maxwell's equations for a geometrical model that replicates the real geometry as much as possible. Such approaches are well suited for industrial processes, for which the CAD models are prior inputs. Nevertheless, we have noticed in many of the results displayed in this article that the system response waveforms are very close to R, L, C circuit waveforms. This is particularly true because the lightning waveforms can barely excite the resonances of most of the systems under consideration. Of course, the main difficulty remains in determining the R, L and C parameters, which is almost not achievable on a complex system.

In the French Industry sponsored program called "PREFACE", such models have been investigated under the generic name of Partial Element Electrical Circuit (PEEC) methods [58]. Particular interest has been given to the so called "stick models", in which 3D structures are represented by wires supporting the circulation of currents. Each wire has a resistance and a radius that allow the determination of its self-inductance. In addition, mutual inductances are calculated analytically, as a function of the respective positions of the wires in the 3D geometry [59]. Then, the entire current response can be obtained by solving the equivalent circuit, either in the frequency or time domain (LIRIC computer code from Onera).

In [60], in order to demonstrate the capability of the approach, an A320 landing gear is modeled with such a stick model. The results are compared to measurements and a full 3D modeling performed with Onera's ALICE FDTD code. The test configuration consists in injecting an A-waveform with a lower level (all of the results are then normalized to the regular 200 kA). On the one hand, figure 19-a shows the structured 5mm-cell mesh used for the ALICE calculation. The entire mesh was made of 80 millions of cells; the time step required by the stability criterion was 25μs which led to a 15-hours total calculation time on 380 processors for passing 20% of the maximum of the response waveform. On the other hand, the equivalent stick model is shown in figure 19-b. Each constituent of the landing gear has been modeled by a wire with an equivalent radius and an equivalent length: in total, there are 56 wires and 40 connections between them. The LIRIC calculation took only a few minutes to calculate the entire signal damped to zero for long times. The advantage of such an approach clearly resides in its short calculation time, which is well suited for parameter analysis and thereby for design optimization.

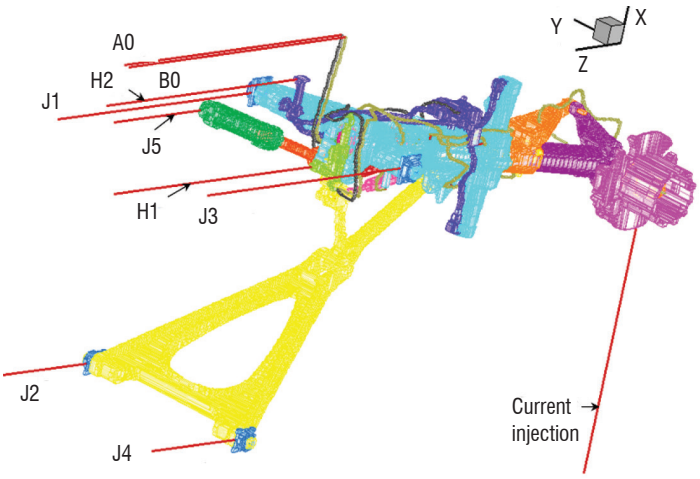

a) FDTD model

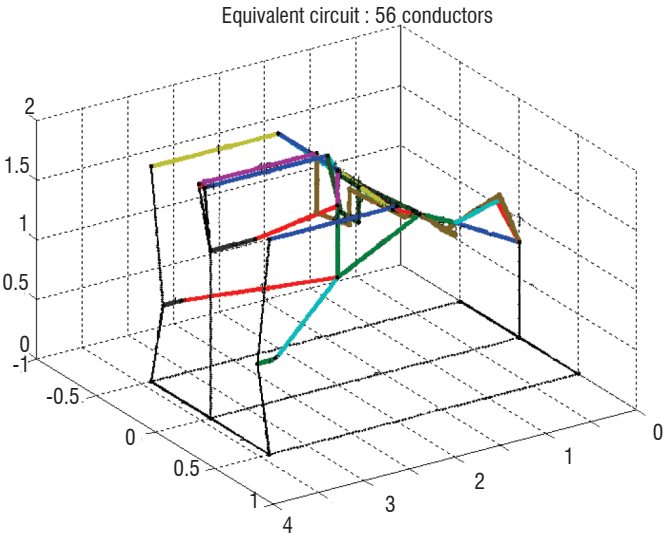

b) Stick model

Figure 19 - Models for a current injection on an A320 landing gear [60]- Courtesy of the PREFACE project

Figure 20-a shows some results obtained for the wires used to close the circuit and for shielded cables (Jx, A0 and B0 – see figure 19). Figure 20-b shows a histogram of the results of the maximum currents obtained. They first show the confidence that can be given in both modeling techniques.

Nevertheless, note that to obtain these results, either by the 3D computer code or by the stick model code, the model is significantly dependent on the values of the contact resistances between constitutive parts; these resistances had to be measured and introduced into the models. Without them, none of the models would have given the expected results.

Of course, in [60], the structure being modeled is mainly made up of a network of bars and more validations must be made for more 3D shapes, in which some 3D surfaces need to be modeled by sets of parallel wires. Nevertheless, considering the quality of the results shown in § "Cables inside and outside a realistic structure", based on the use of 2D invariant cross-sections meshed with parallel wires, there is no reason why such an extension in 3D should not give good satisfactory results. Stick models have been known for a long time. In the 80s they were the precursors of 3D full-wave models and they were used because of their low computation cost [25]. Then, the

trend to reach higher frequencies such as EMP made them become inappropriate and led to the race towards achieving increasingly efficient 3D full wave models. However, this made the numerical modeling community forget how those techniques may be efficient at low frequencies! By the way, such techniques are fast because the model itself introduces some hypotheses on the solution, by imposing the direction of the currents.

Such models are not ready to be introduced in industrial processes yet, as for some 3D full-wave calculations, but there is a good chance that the stick model approach can become part of this overall modeling process in the near future. Indeed, we can foresee a very efficient combination of these two types of full-wave and stick models:

- full wave models may be required for the first calculation, which provides reference results for mapping the current redistribution. They provide a reference calculation;
- then, the stick model decomposition can be made from this first 3D evaluation. It offers the capacity of running sensitivity analyses.

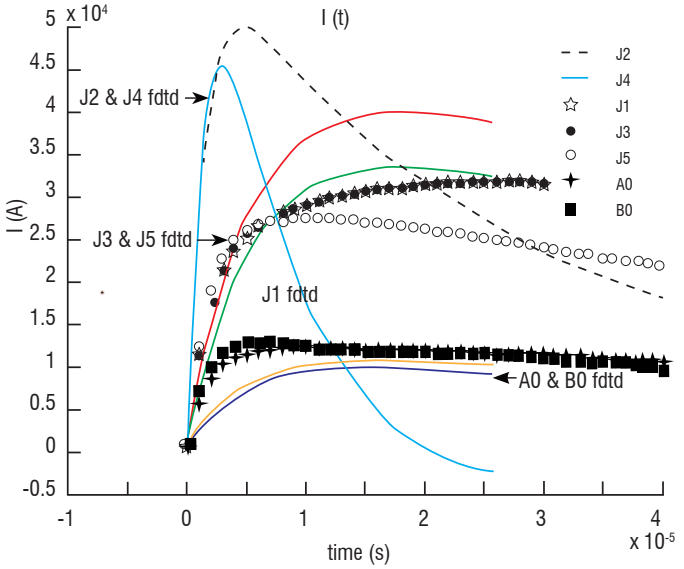

a – Global time domain waveforms

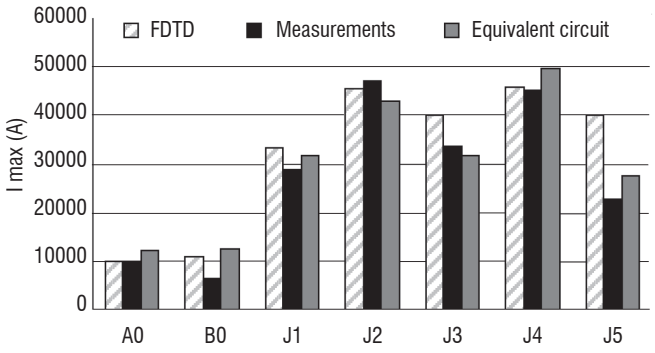

b – Maximum of the waveforms

Figure 20 - Current results on the A320 landing gear (PREFACE project) [60]

Conclusion

In this paper, we have shown that, as for direct lightning, is was impossible to consider addressing the full indirect lightning sequence and lightning analysis must be broken down into a series of independent waveforms, among which type A waveforms are the most relevant for the system, because of their energy content. This is why most of the illustrations in this paper concern this particular waveform of interest.

The elementary coupling effects are of two types: the conduction effect, which merges resistance and inductance effects on induced current lines and the scattering effect, which concerns the EM field produced through local geometries, such as apertures or junctions. Again, the electrical nature of the materials involved in this scattering is very influent on the signature of the resulting attenuation. A very important result is that, most of the time, scattering dominates against diffusion in lossy materials in closed structures, as soon as apertures are made in the structure. This analysis allows the introduction of the concept of EM shield, for which we showed that magnetic shielding was the most difficult to carry out, as far as in direct lightning is concerned, because of its low frequency content.

At system level, the analysis of the structure response is not sufficient and the electrical system response must be investigated. We showed that typical time domain responses could be reproduced by 2D invariant models and that an equivalent source model including generator and impedance could be deduced. We have seen that, for low frequency type-A waveforms, the common coupling was the most significant and could lead to the generation of significantly high amplitude voltage or current signals on cables. In addition, linear approximation is a convenient approximation, because it prevents us from considering non-linear effects, which are so difficult to control from one configuration of injection to the other. Hopefully, we illustrated through real aircraft measurements that this approximation is quite satisfactory, in the sense that it remains conservative on the levels of currents observed in cables.

Two main techniques can be used for protection against indirect lightning. One consists in acting on the installation design, in order to have EM shields contributing to block the magnetic field as much as possible and, therefore, the EM coupling on cables. The key idea to remember is that magnetic shielding requires currents to flow over surfaces as much as possible, otherwise there is no shielding effect. The installation of cable shields obeys the same rules exactly, but at the scale of the cable. Grounding and bounding are very important installation rules, in order to make this current flow possible. In addition, at the same time, they provide the confinement of currents in a volume zone, which is a key point for the maintenance and the control of system evolution in the future life of the AC/RC. Nevertheless, active protection at the level of equipment inputs cannot be avoided, because of safety issues. Indeed, topology based rules can be easily broken if new system components come to be installed on the existing system without any awareness of the rules to be applied. In addition, it must also be said that, due to the system complexity and other constraints naturally not compatible with electromagnetics (think of thermics which requires opening as many apertures as possible to evacuate heat!), perfect EM design rules are not applicable.

Finally, we have shown that EM modeling constantly makes progress, which makes it nowadays a valuable complement to scale-one tests. Nowadays, progress in the 3D modeling of indirect lightning effects is aimed towards two opposite directions: one relies on a very accurate description of the system for applying 3D full-wave solvers; the other relies on intensive simplification, introducing knowledge of the solution on the current distribution in the model as much as possible for applying light solvers, such as electrical circuit solvers. The parallel evolution of the geometrical and electrical aided design tools now

makes it possible to feed the numerical models with the relevant data required by the 3D simulation. However, some of the driving models remain very specific to a given installation and the parameters to put in the models remain inaccessible without measurements. This leads to a new way of thinking for scale-one models: to not consider them only to simulate an effect, but also to provide the model with the missing information, applying very specific configurations designed to measure the model parameters. The advantage is that, once validated, it offers more flexibility and a greater variety of injection configurations than scale-one tests.

Consequently, as a general conclusion, we can say that even if indirect lightning remains a real threat for aircraft, for which constant progress allows a better design of AC/RC to resist this threat, we must ask ourselves if the new emerging aircraft designs will not require some ways of thinking about indirect lightning to be changed. Over the past ten years, we have already seen how the trend towards full composite aircraft has imposed new design rules for allowing the dissipation of currents with new structures, because the surface could not do it properly like the metallic structure did previously. Now comes the trend toward the full electrical aircraft, which of course raises the question of the vulnerability of those new systems to indirect lightning. Because more electrical systems will have to be installed outside the surface of the structure, direct and indirect effects must be handled simultaneously, if the protection is to be properly designed. For example, new embedded de-icing systems must apply the same level of protection and surveillance as antennas. Consequently, the real question is: do we have the knowledge, the rules, the tools and the methodology for making these new systems comply with indirect lightning constraints?

Acknowledgements

The authors would like to thank:
- M. P. Foutrel from SAGEM Defence for having accepted the publication of the animation of the lightning current distribution on the AASM system
- MM. F. Tristant from Dassault and E. Perrin from XLIM for having made possible the publication of figure B6-1.
- M. C. Lair from SNECMA for having accepted the publication of figure 18

References

[1] E. WILLIAMS, S. HECKMAN - *Specific Behaviour of Positive and Negative Atmospheric Electrical Discharges*. Aerospace Lab Issue 5, December 2012
[2] *User's Manual for Certification of Aircraft Electrical/Electronic Systems Against the Indirect Effects of Lightning.* SAE International, 2001-08-01
[3] *Certification of Aircraft Electrical/Electronic Systems for the Indirect Effects of Lightning.* EUROCAE, Issued in May 1996 - Including Amendment N°1 August 1999
[4]RTCA / DO-160 E - *Environment conditions and test procedures for airborne equipment – section 22: lightning induced transient susceptibility*. RTCA Inc, December 2004
[5] *Lightning Aircraft Lightning Environment and Related Test Waveforms Standard.* EUROCAE,1997
[6] P. LAROCHE, P. BLANCHET, A. DELANNOY, F. ISSAC - *Experimental Studies of Lightning Strike to Aircraft.* Aerospace Lab Issue 5, December 2012
[7] J. GRANDO, X. FERRIÈRES, D. MULLER - *Code Alice: Introduction des joints résistifs et exploitation Transall.* Rapport Technique Onera, N° 4/6161 PN, Juin 1992. In French.
[8] V. GOBIN - *Diffraction par les ouvertures et par des objets tridimensionnels. Application à la mesure des impédances de surface des matériaux bons conducteurs*. Thèse de doctorat de 3ème cycle de l'Université de Lille III, juillet 1989. In French.
[9] C. CUILLER, J-C. ALBOUY - *Etude des effets indirects de la foudre sur une voilure réalisée en composite de carbone.* Proceedings of the 1992 French Conference on EMC, CEM 92, 3-4 June 1992, pp. 477-483. In French
[10] J.P. MARQUE, S. BERTUOL, J.P. PARMANTIER - *Modélisation et analyse de l'environnement électromagnétique induit par un foudroiement. Fonctions de transfert d'un réseau de câbles complexes*. Actes du 9ème congrès CEM. Brest, pp. B4-5-B4-10, 8-12 June 1998, in French.
[11] J. PARMANTIER, J. MARQUE, S. BERTUOL, U. THIBBLIN, and al. - *Modeling and Analysis of the Electromagnetic Environment on Aircraft and Helicopter Part 2: Coupling to Complex Cable Networks.* SAE Technical Paper 1999-01-2356, 1999, doi:10.4271/1999-01-2356.
[12] M. RENARD and al. - *Aircraft Electromagnetic Vulnerability Operative Model (MOVEA).* ICOLSE, 28-31 August 2007, paper PPR-52.
[13] L.CHEMARTIN, P.LALANDE, B.PEYROU,A.CHAZOTTES, C.DELALONDRE, B.G.CHÉRON, F.LAGO - *The Thermo Electrical effects of Lightning on Aircraft Structure: Observation and Modeling of Thermo Electro Mechanical Damaging*. Aerospace Lab Issue 5, December 2012
[14] *Aircraft Lightning Environment and Related Test Waveforms.* SAE International, Revision A, 2005-02-21
[15] *Environmental Conditions and Test Procedures for Aircraft Systems.* Version D, Chapters 22 and 23, 2006
[16] P. DEGAUQUE, J. HAMELIN - *Electromagnetic Compatibility*. Oxford, Oxford University Press, Oxford [England]; New York: Oxford University Press, 1993
[17] D.MORGAN, C.J. HARDWICK, S.J. HAIGH, A.J. MEAKINS - *Lightning Test of Aircraft: challenge and issues.* Aerospace Lab Issue 5, December 2012
[18] *Aircraft Lightning Test Methods.* Revision A, SAE International, 2005-03-17
[19] *Protection against lightning*. 2010.
[20] S. RAMO, S. WHINNERY, J.R. VAN DUZER - *Fields and waves in communication electronics.* John Wiley & Sons, 1965, 1984, 1994
[21] P.LALANDE, A.DELANNOY - *The Global Zoning.* Aerospace Lab Issue 5, December 2012
[22] *Aircraft Lightning Zoning.* Revision A, SAE International, 2005-02-16
[23] P. FOUTREL - *« Méthodologie de conception CEM d'un système avionique.* 13th International French Conference on EMC, CEM 2006, 4-6 April 2006.
[24] M.A. BETHE - *Theory of diffraction by small holes*. Phys. Rev 2nd Series 7 and 8.. 1 and 15 October 1944
[25] K.S.H. LEE - *EMP Interaction: principles.* techniques and reference data, Hemisphere Publishing Corporation, Washington, New York, London, 1986.

[26] V. GOBIN, J-P. PARMANTIER - *Chapter 3: Pénétration et couplage dans les structures tridimensionnelles*. In EM Compatibility, Collection technique et scientifique des télécommunications. Lavoisier, Hermes. Paris 2007, under the direction of P. Degauque and A. Zeddam. In French.
[27] K.F. CASEY - *Quasistatic electromagnetic penetration of a mesh-loaded circular aperture*. Interaction notes, note 387, 7 March 1980*.
[28] K.F. CASEY - *Low frequency electromagnetic penetration of loaded apertures*. IEEE Trans. Elect. Compt. Vo1.EMC-23, pp.367-377, 1981.
[29] W. H. HAYT, J. A. BUCK. *Engineering Electromagnetics*. Mc Graw Hill. 2001. Boston, New York, San Francisco, St Louis, (6th edition)
[30] V. GOBIN, J.P. APARICIO, J. GRANDO, J.C. ALLIOT - *The surface impedance: a pertinent parameter to describe finite conductivity materials in numerical codes.* Electromagnetic compatibility (EMC) Symposium, ZURICH, 12-14 mars 1991
[31] F.M. TESCHE, M.V. IANOZ, T. KARLSSON - *EMC Analysis Methods and Computational Models.* John Wiley & Sons, pp.247-266. 1997.
[32][ISS 2008] F. ISSAC - *PEA MOVEA Sous-tâche 1.3 – Fiche E3 – Dimensionnement des termes sources en BF et HF. Approche Onera*. Onera's internal report MOVEA/Onera/E3/08.2-B, 15 December 2008
[33] Y. LE-GOLVAN, G. PENSEC, D. QUILTU, J-P. PARMANTIER*, X. FERRIÈRES*, E. BACHELIER*, S. BERTUOL* - *Etude du couplage d'une onde foudre de type A sur une goulotte de descente de câbles installée à l'intérieur d'une mature intégrée pour navires militaire.* CEM France, Saint-Malo 2006, in French
[34] C. E. BAUM - *The Theory of the Electromagnetic Interference Control.* Interaction Notes. Note 478, December 1989* and, Modern Radio Science 1990, pp. 87-101, Oxford University Press
[35] F. ISSAC, E. BACHELIER, D. PROST, V. ENJALBERT, L. MOHEDANO - *Space launching site protection against lightning hazard.* Special Issue N° xx, "Lightning hazards to Aircraft and Launchers", December 2012
[36] P. DEGAUQUE, J-P. PARMANTIER - *Chapter 2: Couplage aux structures filaires.* in Compatibilité Electromagnétique, Collection technique et scientifique des télécommunications. Lavoisier, Hermes. Paris 2007, under the direction of P. Degauque and A. Zeddam.
[37] E.F. VANCE - *Coupling to Cables*. Wiley Interscience Publication. 1978
[38] M. D'AMORE, M. SARTO, A. SCARLATTI - *Radiated Susceptibility of Wiring System Aboard Lightning Struck Aircraft. Part I: sensitivity to the p.u.l. length external parameters.* Proc. 2002 IEEE Int. Symp. EMC, Minneapolis, MN, August 2002
[39] M. D'AMORE, M. SARTO, A. SCARLATTI - *Radiated Susceptibility of Wiring System Aboard Lightning Struck Aircraft. Part II: sensitivity to the distributed sources.* Proc. 2002 IEEE Int. Symp. EMC, Minneapolis, MN, August 2002
[40] M. APRA, M. D'AMORE, M. SARTO, V. VOLPI - *Lightning Indirect Effects Certification of a Transport Aircraft by Numerical Simulation.* IEEE Transactions on Electromagnetic Compatibility 50(3), pp.513, 2008.
[41] *Guide to Certification of Aircraft in a High Intensity Radiated Field (HIRF) Environment*. version A, EUROCAE, July 2010
[42] http://www.hirf-se.eu/hirf/
[43] J-P. PARMANTIER - *Numerical Coupling Models for Complex Systems and Results*. IEEE Trans. on EMC, vol 46, n°3, pp. 3594, 367 , November 2004.
[44] C. E. BAUM, T. K. LIÙ, F. M. TESCHE - *On the Analysis of General Multiconductor Transmission-Line Networks.* Interaction Notes, Note 350, novembre 1978 Interactions Notes are available at: http://www.ece.unm.edu/summa/notes
[45] C.R. PAUL - *Analysis of Multiconductor Transmission Lines*. New-York: John Wiley & Sons, 1994
[46] L. PALETTA, J-P. PARMANTIER, F. ISSAC, P. DUMAS, J.-C. ALLIOT - *Susceptibility Analysis of Wiring in a Complex System Combining a 3-D Solver and a Transmission-Line Network Simulation.* IEEE Trans. on EMC, Vol. 44, No. 2, pp. 309-317. May 2002.
[47] X. FERRIÈRES, J.P. PARMANTIER, S. BERTUOL, A.R. RUDDLE - *Modeling EM Coupling onto Vehicle Wiring Based on the Combination of a Hybrid FV/FDTD Method and a Cable Network Method.* Proc. of 15th International Zurich EMC Symposium, Zurich, février 2003, pp.465–470
[48] J.-P. BERENGER - *A Perfectly Matched Layer for the Absorption of Electromagnetic Waves*. Journal of Computational Physics, 114(2):185–200, 1994.
[49] J.P. BÉRENGER - *Improved PML for the FDTD Solution of Wave-structure Interaction Problems*. IEEE transactions on Antennas and Propagation, 45(3): pp. 466-473, mars 1997.
[50] J-P. PARMANTIER, S. BERTUOL, T. VOLPERT, C. LAIR, P. DUPRÉ, F. THEROND, G. GUTIERREZ, J.I. PLAZA GOMEZ - *Méthodologie de modélisation/simulation 3D des effets EM d'une injection foudre sur le moteur TP400.* 15th international French conference on EMC, CEM 2010, Limoges, 7-9 April 2010, in French
[51] W. L. KO, R. MITTRA - *A Combination of FD-TD and Prony's Methods for Analyzing Microwave Integrated Circuits.* IEEE Trans. On Microwave Theory and Techniques, VOL. 39, n°12, December 1991
[52] http://plasma-gate.weizmann.ac.il/Grace/
[53] E. PERRIN, C. GUIFFAUT, A. REINEIX, F. TRISTANT - U*sing Transfer Function Calculation and Extrapolation to Improve the Efficiency of the Finite-Difference Time-Domain Method at Low Frequencies.* IEEE Transactions on ElectroMagnetic Compatibility, 52(1), pp. 173, 2010.
[54] E. PERRIN - *Modélisation des effets inirects de la foudre sur avion composite.* Ph. D. report of the University of Limoges, 5 May 2012. In French.
[55] T. K. SARKAR, O. PEREIRA - *Using the Matrix Pencil Method to Estimate the Parameters of a sum of Complex Exponentials*. IEEE Antennas and Propagation Magazine, 37:48–55, 1995
[56] R. HOLLAND, L. SIMPSON - *Finite Difference Analysis of EMP Coupling to Thin Structures and Wires*. IEEE Transactions on ElectroMagnetic Compatibility, 23:88–89, 1981.
[57] R. L. RECHTSCHAFFNER - *Saturated Fraction of 2n and 3n Factorial Designs*. Technometrics, 9:569–575, 1967
[58] A. E. RUEHLI, G. ANTONINI - *The Partial Element Equivalent Circuit (PEEC) Method: Part I: General Overview and Part II: Advanced Modeling.* 16th International Zurich Symposium on EMC, Zurich 13-18 février, Switzerland, 2005
[59] A. RUEHLI, C. R. PAUL, K. GARETT - *Inductance Calculations using Partial Inductances and Macromodels.* 1995 IEEE International Symposium on Electromagnetic Compatibility, pp. 23-28, 1995
[60] D. PROST, F. ISSAC, W. QUENUM, J.P. PARMANTIER - *Lightning Induced Current Simulation using RL Equivalent Circuit: Application to an Aircraft Sub-system Design.* IEEE Trans. On EMC, To be published 2012

Acronyms

2D	(Two-dimensional)
3D	(Three-dimensional)
AC/RC	(Aircraft/Rotorcraft)
CAD	(Conception Assisted Design)
EM	(Electromagnetic)
EFIE	(Electric Field Integral Equation)
EMC	(Electromagnetic Compatibility)
EU	(European Union)
MP	(Matrix Pencil)
p.u.l.	(Per Unit Length)
SEM	(Singularity Expansion Techniques)
SILI	(Short Impulse to Large Impulse)
VCC	(Carbon Composite Wing (Voilure Composite Carbone))

AUTHORS

Jean-Philippe Parmantier obtained his engineering degree from SUPELEC in 1987. In 1988, he joined Dassault Aviation, where he obtained his Ph.D in Electromagnetic Topology from Lille University, in cooperation with The French Aerospace Lab, Onera, France and established the first basis of the CRIPTE code. In 1991, he joined Onera, where he began to apply his research to various complex systems, such as, for example, the EMPTAC test bed aircraft from 1993 to 1996. Since 1999, he has been the head of a Research Group on EMC at Onera; Toulouse, France. He is author and co-author of numerous papers on EMC and the organizer of various EMC related conferences and research projects.

François Issac obtained his Technical University Degree (DUT) in physics measurement in 1982, in Montpellier, France. He began working at Ecopol from 1983 to 1986 on lightning effects and he joined the Office National d'Etudes et de Recherches Aérospatiales (Onera) where he became involved in numerous large scale EMC experiments (in-flight lightning tests on a Transall aircraft in 1987 1990; EMPTAC tests on EM Topology, 1993-1996; joint cooperation on mode stirred chambers with DERA, 1999-2000). Nowadays, his field of interest covers a large area, from low frequency to high frequency, mainly from an experimental point of view. He is co-author of numerous papers dealing with EM measurement validations carried out at Onera.

Vincent Gobin obtained his engineering degree from SUPELEC in 1985. In 1987, he joined Dassault Aviation, where he obtained his Ph.D in Electromagnetic Modeling of Composite Materials from Lille University, in cooperation with the French Aerospace Lab Onera, France. In 1990, he joined Onera, where he continued to work on the numerical modeling of complex structures and antennas, more specifically on integral equations and a multi-domain approach. Since 2008, he has been the head of a Research Group on EMC at Onera, Toulouse, France, studying antennas, materials and EM modeling.